

AD-A170 224

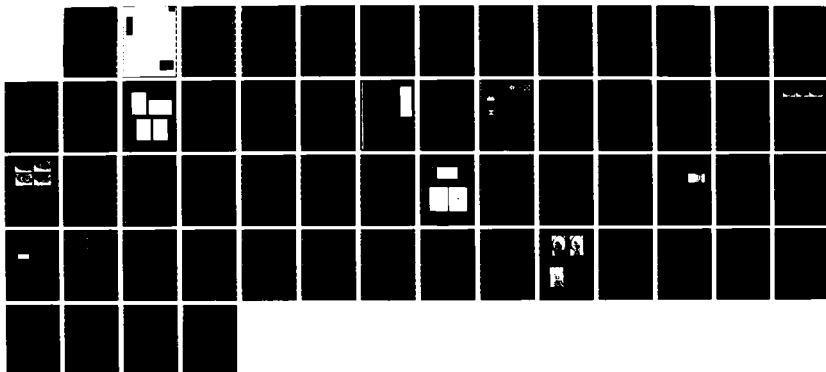
WHITE-LIGHT OPTICAL INFORMATION PROCESSING AND
HOLOGRAPHY(U) PENNSYLVANIA STATE UNIV UNIVERSITY PARK
DEPT OF ELECTRICAL ENGINEERING F T YU 29 JUL 85
AFOSR-TR-86-0483 AFOSR-83-0140

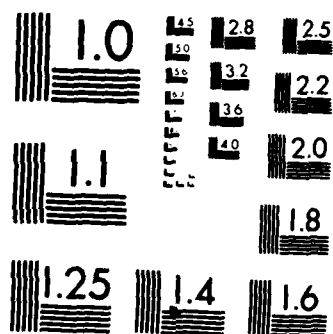
1/1

UNCLASSIFIED

F/G 14/5

NL





MICROCOPY RESOLUTION TEST CHART
NATIONAL BUREAU OF STANDARDS-1963-A

Unclassified

SECURITY CLASSIFICATION OF THIS PAGE

AD-A170 224

i

②

REPORT DOCUMENTATION PAGE

1a. REPORT SECURITY CLASSIFICATION Unclassified			1b. RESTRICTIVE MARKINGS	
SECURITY CLASSIFICATION AUTHORITY			3. DISTRIBUTION/AVAILABILITY OF REPORT Unlimited	
DECLASSIFICATION/DOWNGRADING SCHEDULE				
PERFORMING ORGANIZATION REPORT NUMBER(S)			5. MONITORING ORGANIZATION REPORT NUMBER(S)	
6a. NAME OF PERFORMING ORGANIZATION Electrical Engineering Dept. Pennsylvania State University		6b. OFFICE SYMBOL (If applicable)	7a. NAME OF MONITORING ORGANIZATION Dr. Robert W. Carter, Jr. AFOSR	
6c. ADDRESS (City, State and ZIP Code) University Park, PA 16802		7b. ADDRESS (City, State and ZIP Code) Building 410 Bolling Air Force Base Washington, D.C. 20332		
8a. NAME OF FUNDING/SPONSORING ORGANIZATION AFOSR/NE		8b. OFFICE SYMBOL (If applicable)	9. PROCUREMENT INSTRUMENT IDENTIFICATION NUMBER AFOSR-83-0140	
8c. ADDRESS (City, State and ZIP Code) Building 410 Bolling Air Force Base Washington, D.C. 20332		10. SOURCE OF FUNDING NOS.		
11. TITLE (Include Security Classification) WHITE LIGHT OPTICAL PROCESSING AND HOLOGRAPHY		PROGRAM ELEMENT NO. 611025	PROJECT NO. 2305	TASK NO. B1
12. PERSONAL AUTHOR(S) Yu, Francis Tiong-Suy				
13a. TYPE OF REPORT Annual Report		13b. TIME COVERED FROM 3/15/84 TO 5/14/85	14. DATE OF REPORT (Yr., Mo., Day) 1985, July, 29	
15. PAGE COUNT 53				
16. SUPPLEMENTARY NOTATION				
17. COSATI CODES			18. SUBJECT TERMS (Continue on reverse if necessary and identify by block number)	
FIELD	GROUP	SUB. GR.	White-light processing, solar-light processing, processing with Magneto optic, noise measurement, white-light Fourier holography, generation of speech spectrogram, color image processing.	
19. ABSTRACT (Continue on reverse if necessary and identify by block number) During the fourth year (FY'84), major progress has been made on the white-light optical signal processing and holographic research program. In this period we have explored the possibility of using natural solar-light for image processing. The advantage of this technique is the processing system does not require to carry its own light source. It is very suitable for spaceborne and satellite application. We have also developed a technique of measuring the noise performance of a white-light processor. The results confirm well with the analytical predictions. We have applied a programmable Magneto-optic spatial light modulator for white-light signal processing. We have shown that the MOSLM responds to polarized light, in which offers the advantage of color coding signal processing. The most important of this device must be the programmability, for which a real-time programmable optical processor can be in principle realized in practice. We have, in this period, also developed a technique of generating a Fourier transform hologram with a white-light source. This technique is very suitable for reconstructing color hologram images				
20. DISTRIBUTION/AVAILABILITY OF ABSTRACT UNCLASSIFIED/UNLIMITED <input checked="" type="checkbox"/> SAME AS RPT. <input type="checkbox"/> DTIC USERS <input type="checkbox"/>			21. ABSTRACT SECURITY CLASSIFICATION Unclassified	
22a. NAME OF RESPONSIBLE INDIVIDUAL Lt Col Carter		22b. TELEPHONE NUMBER (Include Area Code) 202 767-4931	22c. OFFICE SYMBOL AFOSR/NE	

DTIC
ELECTED
JUL 28 1986
E

Unclassified

SECURITY CLASSIFICATION OF THIS PAGE

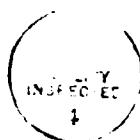
with white-light processing. We have also recently developed a technique of generating a spatial-frequency color coded speech spectrogram with a white-light optical system. This system not only offers a low-cost alternative but also eliminated the complicated programming procedure with digital counterpart. Moreover, the multicolor display is more sensitive for human-visual perception and discrimination. In this period, we have also developed a spatial encoding technique for color image retrieval so that the annoying moire fringes can be eliminated. In short, we have once again demonstrated the versatility of the white-light progress system; a wide variety of signal processings can be easily achieved with very cost effectiveness and high efficiency.

Table of Contents

	<u>Page No.</u>
Abstract	1
I. Introduction	1
II. Summary and Overview	1
2.1 Solar-Light Optical Signal Processing	2
2.2 White-Light Processing with Magneto-Optic Device	2
2.3 Measurement of Noise Performance	3
2.4 White-Light Fourier Holography	3
2.5 Optical Generation of Speech Spectrogram with White-Light Source	3
2.6 Progress on Archival Color Film Storage	4
2.7 An Invited Chapter of a Book	4
2.8 Remark	5
2.9 Future Research	5
2.10 References	7
III. Solar-Light Optical Processing	8
IV. White-Light Processing with Magneto-Optic Device	13
V. Measurement of Noise Performance	19
VI. White-Light Fourier Holography	26
VII. Optical Generation of Speech Spectrogram	32
VIII. Progress on Archival Color Film Storage	39
IX. Recent Advances on White-Light Image Processing	47
X. List of Publications Resulting from AFOSR Support	50

Accession For	
NTIS GRA&I	<input checked="" type="checkbox"/>
DTIC TAB	<input type="checkbox"/>
Unannounced	<input type="checkbox"/>
Justification	
By	
Distribution/	
Availability Codes	
Dist	Avail and/or Special
A-1	

AIR FORCE OFFICE OF SCIENTIFIC RESEARCH (AFSC)
 NOTICE OF TRANSMITTAL TO DTIC
 This technical report has been reviewed and is
 approved for public release IAW AFR 190-12.
 Distribution is unlimited.
 MATTHEW J. KERPER
 Chief, Technical Information Division



I. Introduction

We have, in the past fourteen-month period, completed several major research programs in the supported area on white-light optical signal processing and holography. The performances of our tasks done were very consistent with proposed research programs supported by Air Force Office of Scientific Research Grant No. AFOSR-83-0140. Several results, in part, have been published in various open technical journals and have been presented in scientific conferences. Sample copies of these papers are included in this annual report in the subsequent sections, to provide a concise documentation of our research program. In the following sections, we shall give an overview of our research work done in the period from March 15, 1984 to May 14, 1985. We shall detail some of those accomplished works. A list of publications resulting from this support is included at the end of this report.

II. Summary and Overview

The advances of quantum electronics have brought into use the infrared and visible range of electromagnetic wave. The investigation of intensive coherent light sources has permitted us to build more efficient optical systems for communication and signal processing. However coherent optical systems are plagued with coherent artifact noise, which frequently limits their processing capability. However, this difficulty has prompted us to look at optical processing from a new standpoint, and to consider whether it is necessary for all optical processing operations to be carried out by pure coherent sources. We have found that many optical processings can be carried out either by partially coherent source or white-light source. The advantages of white-light processings are: (1) It can suppress the coherent artifact noise; (2) the white-light sources are usually inexpensive; (3)

the processing environment is generally very relaxed; (4) the white-light system is relatively easy and economical to operate; and (5) the white-light processor is particularly suitable for color image processing.

In the following sections, we shall highlight some of the research done during the period from March 15, 1984 to May 14, 1985.

2.1 Solar-Light Optical Signal Processing (Section III).

We have in this period performed an experiment of optical signal processing with natural solar light [1]. We have shown that a white-light processor can be easily implemented with natural solar light for optical signal processing. The basic advantage of the solar optical processing is that the processing system does not require to carry an artificial light source, which is very suitable for spaceborne optical processing application. In addition to the simplicity, versatility, polychromaticity, and noise immunity of the white-light processing system, the solar processor is very durable and the operation is very cost effective.

2.2 White-Light Processing with Magneto-Optic Device (Section IV)

We have also in this period performed an application of a magneto-optic spatial light modulator with white-light processing [2]. The spatial light modulator to white-light optical signal processing is presented. We have shown that the magneto-optic device responds to the polarized white light, in which a wide range of color object patterns can be generated. Since the magneto-optic device is a transmitted type spatial light modulator, it is very suitable for real-time programmable spatial filter synthesis and object pattern generation for optical signal processings.

2.3 Measurement of Noise Performance (Section V)

A measurement technique for the noise performance of a white-light optical signal processor is also performed in this period [3]. The technique utilizes a scanning photometer to trace out the output noise intensity fluctuation of the optical system. The effect of noise performance due to noise perturbation at the input and Fourier planes is measured. The experimental results, except for amplitude noise at the input plane, show the claims for better noise immunity, if the optical system is operating in the partially coherent regime. We have also measured the noise performance due to perturbation along the optical axis of the system. The experimental results show that the resulting output SNR improves considerably by increasing the bandwidth and source size of the illuminator. The optimum noise immunity occurs for phase noise at the input and output planes. For amplitude noise, the optimum SNR occurs at the Fourier plane. In brief, the experimental results confirm the analytical results that we recently evaluated.

2.4 White-Light Fourier Holography (Section VI)

In this period we have also developed a technique for generating broad spectral band Fourier holograms with an encoded white light source [4]. Since this technique utilizes primary white-light construction and reconstruction process, it is quite suitable for color Fourier hologram image reconstruction.

2.5 Optical Generation of Speech Spectrogram with White-Light Source (Section VII)

We have also developed a technique of generating speech spectrogram with a white-light optical processor [5]. Since the technique utilizes a

white-light source, the speech spectrograms thus generated are frequency color-coded resulting in easier visual discrimination. The temporal-to-spatial conversion of speech signal is accomplished by means of density modulation with a CRT scanner. The scaling procedure of the speech spectrogram as well as the frequency resolution limit of the system is discussed.

2.6 Progress on Archival Color Film Storage (Section VIII)

In the past fourteen-month period, we have completed an investigation of archival storage of color films with white-light optical processing technique [6]. We have developed a spatially encoding technique such that the moire fringe pattern inherently existing with the retrieved color image can be avoided. To improve the diffraction efficiency of the film, we have introduced a bleaching process so that the step of obtaining a positive encoded transparency can be eliminated. Instead of restricting the encoding processing in the linear region of the T-E curve, we would allow the encoding in the linear region of the D-E curve, so that a broader range of encoding exposure can be utilized. Experimental results indicate that excellent color fidelity, high signal to noise ratio, and good resolution of the reproduced color images can be obtained.

2.7 Contributed an Invited Chapter of a Book (Section IX)

We have also in the past few months published an invited chapter on "Recent Advances in White-Light Image Processing" in the Advances in Electronics and Electron Physics Vol. 63, edited by P. W. Hawkes (Academic Press Inc.) [7]. This chapter illustrated several important color image processing operations can be easily accomplished with white-light processor, for which some of the results can not be obtained with digital techniques at this time. We have acknowledged particularly to the support

of the AFOSR. Without their support, these results could not have been accomplished.

2.8 Remarks

We have also, in this period, investigated a microprocessor based real-time optical signal processing. Interesting results would be surfaced in the near future. In short, the white-light signal processing research program, supported by AFOSR, is conducted extremely well as proposed. As it can be seen, several significant results have been documented in open literature available for the interested technical and research staffs, for example, as listed in Section III to IX.

2.9 Future Research

Our aim in the following years is toward the following goals:

1. To synthesize a low cost microprocessor based white-light pseudocolor encoder.
2. To carry out the white-light programmable pseudocolor encoder for multispectral band satellite pictures, x-ray transparencies, scanning electron micrograph, etc.
3. To develop a real-time programmable processing capability with various spatial-light modulators.
4. To carry out various real-time signal processing applications.
5. To develop a real-time spatial/spectral signal processing capability.
6. Provide experimental demonstrations and applications of the principles and processing operation that we proposed.
7. To develop techniques of synthesizing a broad spectral band complex matched filter for the white-light processing system.

8. To develop a computer generated spatial filters program that is suitable for broad spectral band white-light processing, etc.

2.10 References

1. F. T. S. Yu and X. X. Chen, "Solar Optical Processing," Opt. Commun. 51, 377 (1984).
2. F. T. S. Yu, X. J. Lu and M. F. Cao, "Application of a Magneto-Optic Spatial Light Modulator to White-Light Optical Processing," Appl. Opt., 23, 4100 (1984).
3. F. T. S. Yu, L. N. Zheng and F. K. Hsu, "Measurement of Noise Performance for a White-Light Optical Signal Processor," Appl. Opt., 24, 173 (1985).
4. F. T. S. Yu, X. X. Chen and S. L. Zhuang, "Progress Report on Archival Storage of Color Films Utilizing a White-Light Processing Technique," J. Opt., 16, 59 (1985).
5. F. T. S. Yu, T. W. Lin and K. B. Xu, "White-Light Optical Speech Spectrogram Generation," Appl. Opt., 24, 836 (1985).
6. F. T. S. Yu and F. K. Hsu, "White-Light Fourier Holography," Opt. Commun., 52, 384 (1985).
7. F. T. S. Yu, "Recent Advances in White-Light Image Processing," in Advances in Electronics and Electron Physics, Vol. 63, edited by P. W. Hawkes, Academic Press, New York, 1985.

SECTION III

Solar-Light Optical Processing

SOLAR OPTICAL PROCESSING

F.T.S. YU and X.X. CHEN

*Electrical Engineering Department, The Pennsylvania State University,
University Park, PA 16802, USA*

Received 27 March 1984

We will show that a white-light processor can be easily implemented with natural solar light for optical signal processing. The basic advantage of the solar optical processing is that the processing system does not require to carry an artificial light source, which is very suitable for spaceborne optical processing application. In addition to the simplicity, versatility, polychromaticity, and noise immunity of the white-light processing system, the solar processor is very durable and the operation is very cost effective. Several elementary experimental demonstrations obtained with the solar light processing are given.

1. Introduction

Since the discovery of laser in the earlier 60's, the laser has become an indispensable light source for most of the optical signal processings [1-4]. Aside from the disadvantage of inherent artifact noise, the lasers are generally expensive and in some cases the maintenance of a coherent source could be a problem. Recently we have developed a grating based optical signal processing technique, which can be easily carried out with a broad band white-light source [5]. The major advantages of the white-light processing, as in contrast with the coherent counterpart, are the simplicity, versatility, polychromaticity, cost efficiency and artifact noise immunity.

We will, however, in this paper experimentally demonstrate that several elementary optical image processings can be carried out by solar or sun-light illumination. Since the solar light contains all the visible wavelength, the experimental results that we will show would be in colour images.

2. Color image retrieval

Let us briefly describe a color image retrieval utilizing the solar light. Let us assume that a spatially encoded transmittance of a color object transparency be [6]

$$t(x, y) \approx \exp[iM\{T_r(x, y)[1 + \operatorname{sgn}(\cos p_r y)] + T_b(x, y)[1 + \operatorname{sgn}(\cos p_b x)] + T_g(x, y)[1 + \operatorname{sgn}(\cos p_g x)]\}] \quad (1)$$

where M is an arbitrary constant, T_r , T_b , and T_g are the red, blue, and green image irradiances of the color object, p_r , p_b , and p_g are the respective carrier spatial frequencies, (x, y) is the spatial coordinate system of the encoded film, and

$$\operatorname{sgn}(\cos x) \triangleq \begin{cases} 1, & \cos x \geq 0 \\ -1, & \cos x < 0 \end{cases}$$

If we place the encoded film of eq. (1) at the input plane of a solar optical processor of fig. 1, then the first-order complex wave field at the Fourier plane, for every λ , would be

$$\begin{aligned} S(\alpha, \beta; \lambda) \approx & \hat{T}_r\left(\alpha, \beta \pm \frac{\lambda f}{2\pi} p_r\right) + \hat{T}_b\left(\alpha \pm \frac{\lambda f}{2\pi} p_b, \beta\right) \\ & + \hat{T}_g\left(\alpha \pm \frac{\lambda f}{2\pi} p_g, \beta\right) + \hat{T}_r\left(\alpha, \beta \pm \frac{\lambda f}{2\pi} p_r\right) * \hat{T}_b\left(\alpha \pm \frac{\lambda f}{2\pi} p_b, \beta\right) \\ & + \hat{T}_r\left(\alpha, \beta \pm \frac{\lambda f}{2\pi} p_r\right) * \hat{T}_g\left(\alpha \pm \frac{\lambda f}{2\pi} p_g, \beta\right) \\ & + \hat{T}_b\left(\alpha \pm \frac{\lambda f}{2\pi} p_b, \beta\right) * \hat{T}_g\left(\alpha \pm \frac{\lambda f}{2\pi} p_g, \beta\right), \end{aligned} \quad (2)$$

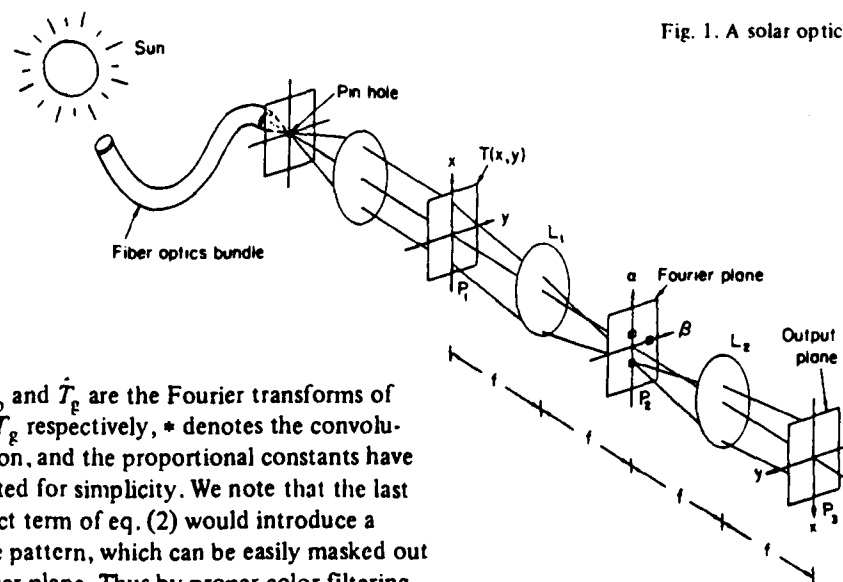


Fig. 1. A solar optical processor.

where \hat{T}_r , \hat{T}_b and \hat{T}_g are the Fourier transforms of T_r , T_b and T_g respectively, $*$ denotes the convolution operation, and the proportional constants have been neglected for simplicity. We note that the last cross product term of eq. (2) would introduce a moiré fringe pattern, which can be easily masked out at the Fourier plane. Thus by proper color filtering the smeared Fourier spectra as illustrated in fig. 1, a true color image can be retrieved at the output image plane p_3 . The corresponding output image irradiance would be

$$I(x, y) = T_r^2(x, y) + T_b^2(x, y) + T_g^2(x, y), \quad (3)$$

which is a superposition of three primary encoded color images. Thus we see that a moiré free color image can be retrieved from a natural solar light.

For experimental demonstration, we show a retrieved color image of fig. 2 obtained from the solar light optical processing. In view of the retrieved color image, we see that the reproduced color image is spectacularly faithful with respect to the original color object and the image contains virtually no coherent artifact noise.

3. Pseudocolor encoding

Most of the optical images obtained in various scientific applications are gray-level density images. For example, scanning electron microscopic images, multispectral band aerial photographic images, X-ray transparencies, infrared scanning images, etc. However, humans can perceive in color better than gray-level variations. Therefore a color coded image can provide a greater ability in visual discrimination.

Let a three-level (i.e., positive, negative and intermediate level) spatially encoding transparency be

$$T(x, y) \approx \exp[iM\{T_1(x, y)[1 + \text{sgn}(\cos p_1 y)] + T_2(x, y)[1 + \text{sgn}(\cos p_2 x)] + T_3(x, y)[1 + \text{sgn}(\cos p_3 x)]\}], \quad (4)$$

where M is an arbitrary constant, T_1 , T_2 , and T_3 are the positive, the negative, and the negative and positive product image exposures, p_1 , p_2 , and p_3 are the respective carrier spatial frequencies.

Again by the insertion of the encoded transparency of eq. (4) at the input plane p_1 of the solar light processor of fig. 1, and by various color filtering of the smeared Fourier spectra in the Fourier plane, a density color coded image can be obtained at the output plane, such as

$$I(x, y) = T_{1r}^2(x, y) + T_{2b}^2(x, y) + T_{3g}^2(x, y),$$

where T_{1r} , T_{2b} , and T_{3g} are the red, blue, and green color intensity distributions of the three spatially encoded images. Thus we see that a density color coded image can be easily obtained with the solar light.

Fig. 3 shows a density pseudocolor encoded X-ray image of a woman's pelvis, obtained with the solar processor of fig. 1. In this color encoded image, the positive image is encoded in red, the negative image is encoded in blue, while the product image is encoded in green. By comparing the pseudocolor coded image with the original X-ray picture, it appears that the soft tissues can be better differentiated by the color coded image.



Fig. 2. A retrieved color image.

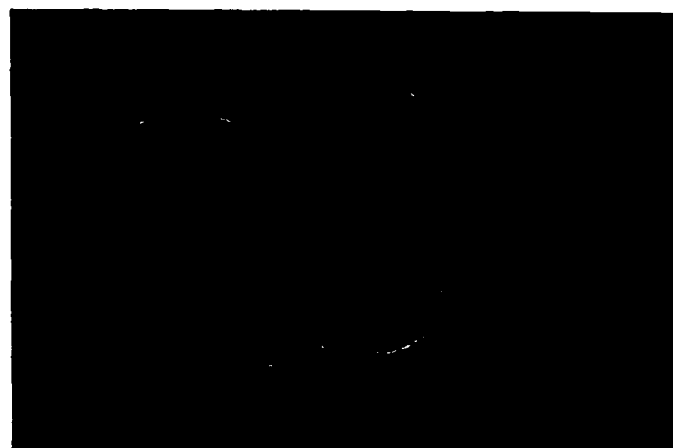


Fig. 3. A density pseudocolor encoded X-ray image.

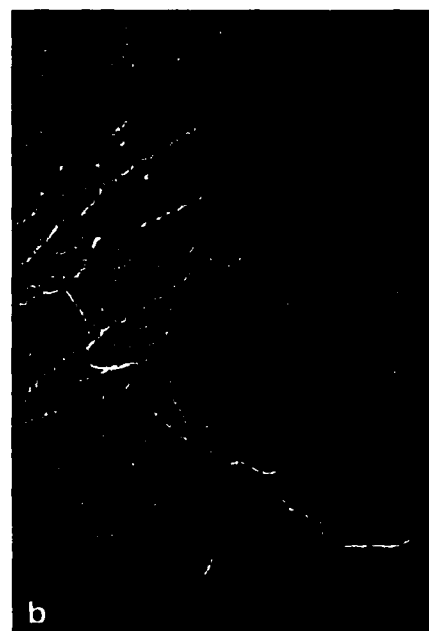
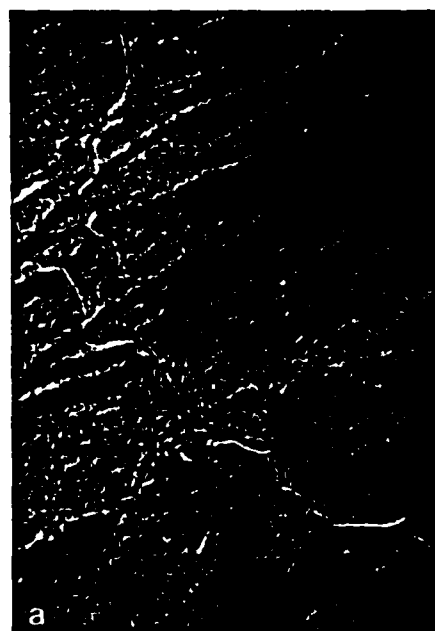


Fig. 4. Samples of false-color Landsat images. (a) Band 4 is encoded in green while band 5 is encoded in red. (b) Band 4 is encoded in green, band 5 is encoded red, and band 7 is encoded blue.

4. As apply to multispectral Landsat images

False-color encoded Landsat images would allow us for the discrimination of various earth surface features. For example, forests agricultural lands, water, urban areas, and strip mines can be shown on the color coded images if each of the thematic image were displayed in a different color. With reference to the spatial encoding method as described previously, a N -spectral band encoded transparency may be described as

$$t(x, y) \approx \exp \left[iM \left(\sum_{n=2k+1}^{N/2} T_n(x, y) [1 + \operatorname{sgn}(\cos p_n y)] + \sum_{n=2k}^{N/2} T_n(x, y) [1 + \operatorname{sgn}(\cos p_n x)] \right) \right], \quad k = 1, 2, \dots, \quad (5)$$

where T_n are the multispectral band image irradiances. We note that the use of the orthogonal samplings (i.e., spatial encoding directions) is to avoid the moiré fringes of the output image. Needless to say that if the encoded film of eq. (5) is inserted at the input plane of the solar optical processor, then false-color encoding can be taken place in Fourier plane. The output false-color coded image irradiances can be shown as

$$I(x, y) = \sum_{n=1}^N T_n^2(x, y; \lambda_n), \quad (6)$$

where T_n^2 represents the irradiance of n th spectral band image and λ_n denotes the corresponding coded color. Thus we see that a false-color coded multispectral image can be easily obtained with the solar light processing.

For simplicity, three bands of multispectral scanner Landsat data were processed for pseudocoloring. These bands were from the blue-green (band 4: 0.5–0.6 μm), red (band 5: 0.6–0.7 μm), and reflected infrared (band 7: 0.8–1.1 μm) spectral regimes. The scene is a 78 X 107 km subsample of Landsat scene showing a section of Susquehanna River Valley in Southeastern Pennsylvania. Fig. 4 shows the results of the false-color coded Landsat data obtained with the solar optical processor of fig. 1. In fig. 4(a) where band 4 is encoded green and band 5 is encoded red, the Susquehanna River and small bodies of water are delineated as deep red. The islands in the Susquehanna River are easily distinguished. Strip mines are dark red, urban areas (Harrisburg) are medium red, and

agricultural lands are light red, orange, and yellow. Forested areas are green. In fig. 4(b), where band 4 is encoded green, band 5 is encoded red, and band 7 is encoded blue, the Susquehanna River appears as violet, and the other bodies of water as shades of blue. The surface mines and urban areas are dark red. The agricultural valleys are orange and the forested regions are green. Thus again we see that false-color coded images can be easily obtained with a solar optical processor.

5. Conclusion

We have demonstrated that a white-light optical processor can also utilize natural solar light for image processing. One of the obvious advantages of the solar light optical processing is that the system does not require to carry its own light source. Thus the proposed solar optical processor is very suitable for spaceborne or satellite optical processing applications. One can image that if an orbiting spaceborne satellite optical processor is required to carry its own light source, for example a powerful laser, then, aside the heavier payload, the question is that how long the light source will last? If one used the natural solar light, we can easily perceive that the optical system would continue to function for a great number of years, possibly beyond the present civilization. Although the development of the solar optical processing is still in the infancy stage however it is not difficult to predict that it would offer many useful applications, particularly to the space communication and signal processing needs.

We wish to acknowledge the support of the US Air Force Office of Scientific Research grant AFOSR-83-0140.

References

- [1] L.J. Cutrona, E.N. Leith, C.J. Paterno and L.J. Porcello, IRE Trans. Inform. Theory, IT-6 (1960) 386.
- [2] A. Vander Lugt, IEEE Trans. Inform. Theory, IT-10 (1964) 139.
- [3] A. Vander Lugt, IEEE Proceedings 62 (1974) 1300.
- [4] F.T.S. Yu, Optical information processing (Wiley-Interscience, New York, 1983).
- [5] F.T.S. Yu, Optics Comm. 27 (1978) 23.
- [6] F.T.S. Yu, X.X. Chen and S.L. Zhuang, Appl. Optics, to be published.
- [7] F.T.S. Yu, X.X. Chen and T.H. Chao, J. Optics, to be published.

SECTION IV

White-Light Processing with Magneto-Optic Device

Application of a magneto-optic spatial light modulator to white-light optical processing

Francis T. S. Yu, Xiaojing Lu, and Miaofu Cao

The application of a programmable magneto-optic spatial light modulator to white-light optical signal processing is presented. We have shown that the magneto-optic device responds to the polarized white light, in which a wide range of color object patterns can be generated. Since the magneto-optic device is a transmitted type spatial light modulator, it is very suitable for real-time programmable spatial filter synthesis and object pattern generation for optical signal processings. Experimental demonstrations of some of the elementary spatial filter syntheses and pseudocolor encodings are provided.

I. Introduction

The recent development of magneto-optic spatial light modulator (also called Light-Mod) has stimulated potential applications to the real-time optical signal processing.^{1,2} The Light-Mod consists of a layer of magnetic iron-garnet thin film deposited on a transparent nonmagnetic substrate. The magnetic thin film is, however, formed into a 2-D array of separated magnetically bistable mesas or pixels. As a plane polarized light transmits through the array of the mesas, the polarization of the mesas can be spatially modulated by magnetically switching through the Faraday effect. Since the Light-Mod is a transparent type device unlike the other spatial light modulators,^{3,4} the device is very suitable for the applications to real-time object pattern generation and spatial filter synthesis.

Because of the cross-array formation of the mesas, the device has a 2-D mesh structure for which the array of mesas or pixels can be switched on and off with an x - y matrix addressed of currents. Thus each pixel of the Light-Mod would take one of the only two possible states, which depends on the direction in which the pixel is magnetized. Thus we see that the Light-Mod is essentially a binary type spatial light modulator (SLM) in contrast with the other SLM.

Since the Light-Mod can be electrically switched, an object pattern can be written on the device with a computer; thus the Light-Mod is also a programmable

spatial light modulator, which is particularly attractive to the application to programmable optical processing.

In this paper we will, however, illustrate some applications of this magneto-optics device to a white-light optical signal processor. We will show that the device is capable of generating various elementary spatial filters and object patterns for optical processings. Since the device would be used in a white-light optical processor, we will first demonstrate the effect of the device under the polarized white-light illumination. We will show that the device responds to a wide range of polarized light, and it is suitable for generating color-coded spatial filters and color-coded object patterns.

II. Effect under White-Light Illumination

We shall first illustrate the effect of spectra distribution under white-light illumination. Since the device is essentially an $n \times m$ array of transparent pixels (or mesas), the Fourier spectra of the device would have a similar distribution to that of a 2-D cross grating. If we insert the Light-Mod in the input plane of a white-light processor, we would expect a set of smeared rainbow color Fourier spectra distributed at the spatial frequency plane. Since the current Light-Mod under test would not respond to wavelengths shorter than the green light, their Fourier spectra would, therefore, only smear from red to green. Nevertheless, this range of spectral lines would provide us with a wide variety of colors for the polychromatic processing.

To simplify our discussion on the effect under the white-light illumination, we provide three simple object patterns of the device, as illustrated in the left-hand column of Fig. 1. The center column is a set of equations to represent the Fourier transforms of these object patterns, where $1/l$ is the spatial frequency of the inherent grating structure of the device, a is the pixel size,

The authors are with Pennsylvania State University, Department of Electrical Engineering, University Park, Pennsylvania 16802.

Received 28 April 1984.

0003-6935/84/224100-05\$02.00/0.

© 1984 Optical Society of America.

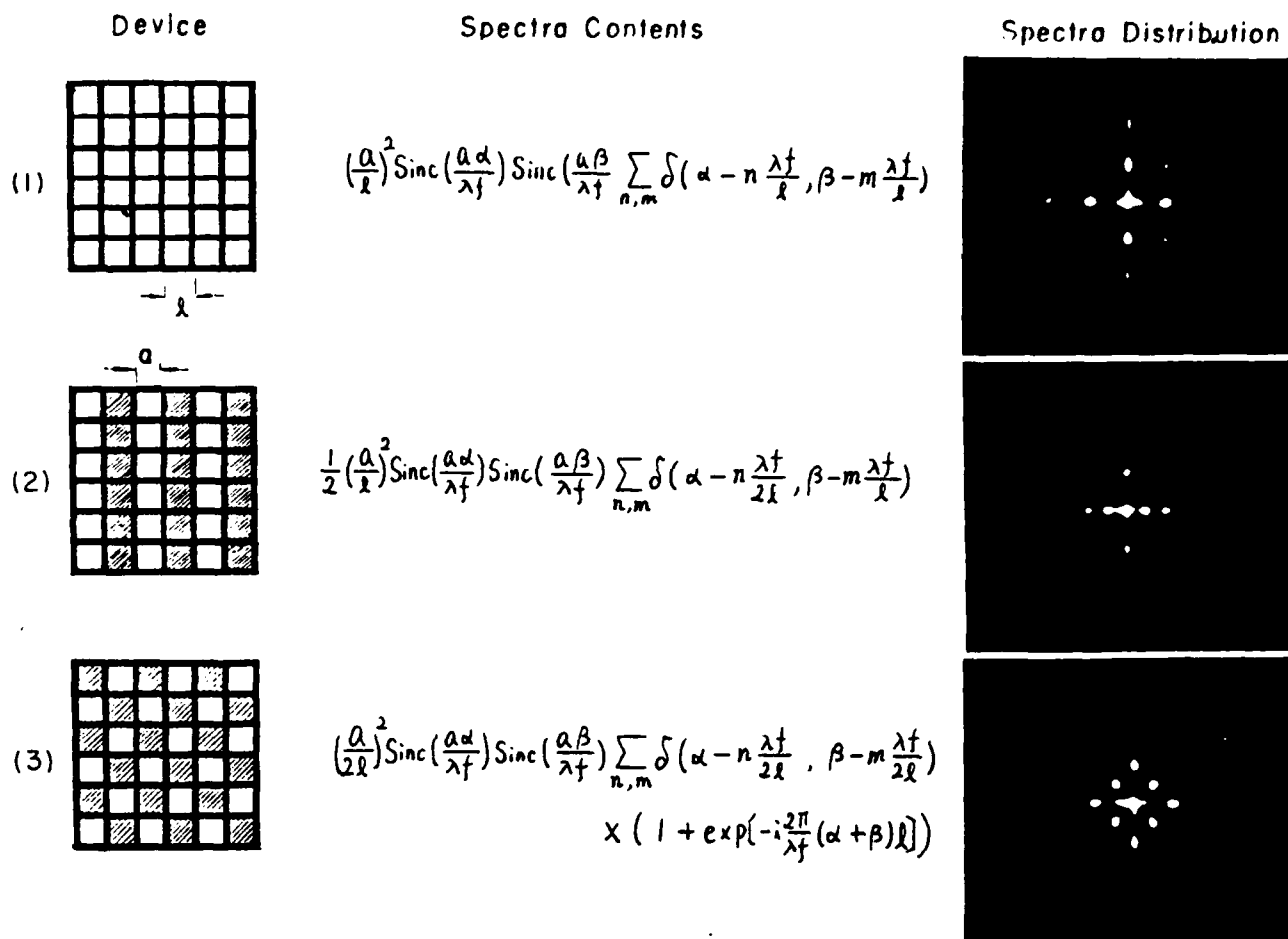


Fig. 1. Elementary patterns of the device and the corresponding smeared Fourier spectra.

λ is the wavelength of illumination, and f is the focal length of the transform lens. The corresponding smeared Fourier spectra distributions are also shown in the right-hand column of the same figure.

Let us now discuss the effect of the device under the polarized white-light illumination. We assume that an object pattern, used either as a spatial filter or as an input object, is generated by the device with a programmable computer. If the device is illuminated by a polarized white-light, one would see the color of the object pattern changes as the direction of the polarization changes. Since the device responds to a broad spectral bandwidth of light from red to green, a wide variety of color object patterns can be generated in which the color characterization of the device is shown in Fig. 2. In this figure the outer region represents the magnetized pixels (i.e., object pattern), and the inner region represents the unmagnetized pixels (i.e., background). For example, if the polarizer is set at $\sim 88^\circ$ angle relative to the vertical axis of the device, the object pattern would be in yellow color, which has the greatest transmittance, while the background would be in black, as can be seen in Fig. 2. If the polarizer is turned slightly counterclockwise, one would see that the object pattern remains in yellow color while the background changes to dark green color (or red color, if the polarizer

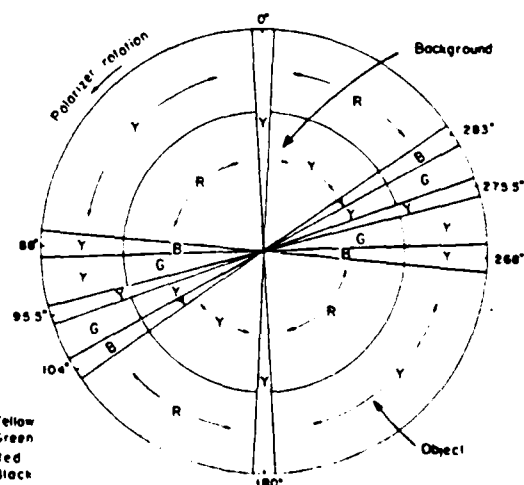


Fig. 2. Color transmittant characteristic of the magnetooptic device under polarized white-light illumination.

is rotated slightly clockwise). If further advancing counterclockwise, the background would become light green while the object pattern still remains in yellow. We further note that, if the polarizer is set at $\sim 104^\circ$, a contrast reverse of the color object pattern appears. If the polarizer is set between 180 and 95.5° , the entire

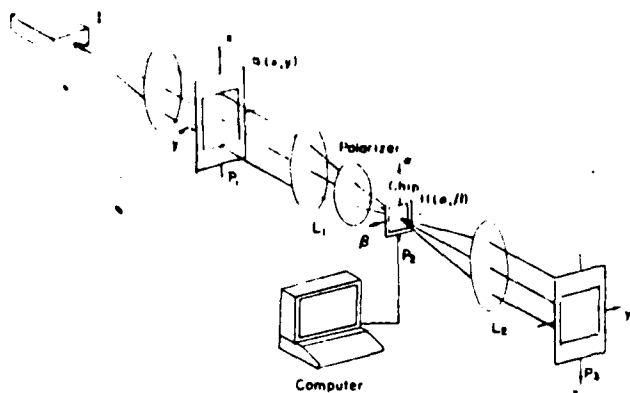


Fig. 3. White-light optical signal processing utilizing a programmable spatial filter: L , white-light source; $H(\alpha, \beta)$, spatial filter generated by the device; L , transform lens.

device would become yellowish, a contrast reverse color pattern would take place for further turning of the polarizer. Moreover, from Fig. 2 we see that the color characterizations of the device are repeated for every rotation of the polarizer. Thus a wide range of color object patterns can be generated for polychromatic signal processing.

III. Elementary Spatial Filtering

We shall now discuss the utilization of the Light-Mod as a programmable spatial filter for a white-light optical processing as shown in Fig. 3. We note that the device is driven by a computer to generate elementary binary spatial filters (e.g., high-pass and wedge filters).

Since the inherent grating structure of the device produces higher-order diffractions (as shown in Fig. 1), the separation of these higher-order signals is depending on the sampling frequency (i.e., the grating structure) of the device, and the spatial frequency content of the arriving complex wave field. In other words, it depends on the pixel size of the device, the frequency content of the object spectra, and the focal length of the transform lens.

We shall now investigate the effect of the output image irradiance due to the device used as a programmable spatial filter. With reference to Fig. 3, the intensity distribution at the output plane can be written as⁵

$$\begin{aligned} \mathcal{F}^{-1}[S(\alpha, \beta; \lambda)H(\alpha, \beta)] &= s(x, y) * h(x, y; \lambda) \\ &= s(x, y) * \sum_{n, m} \left(\frac{a}{l}\right)^2 \text{sinc}\left(\frac{a}{\lambda l}x\right) \text{sinc}\left(\frac{a}{\lambda l}y\right) \delta\left(x - n\frac{\lambda}{l}, y - m\frac{\lambda}{l}\right) \\ &= \left(\frac{a}{l}\right)^2 \sum_{n, m} \text{sinc}\left(n\frac{a}{l}\right) \text{sinc}\left(m\frac{a}{l}\right) s\left(x - n\frac{\lambda}{l}, y - m\frac{\lambda}{l}\right), \end{aligned} \quad (1)$$

where \mathcal{F}^{-1} denotes the inverse Fourier transformation, $*$ represents the convolution operation, $S(\alpha, \beta; \lambda)$ is the Fourier spectrum of the input signal $s(x, y)$, $H(\alpha, \beta)$ is the amplitude transmittance of the device used as a spatial filter, $h(x, y; \lambda)$ is the corresponding impulse response, δ is the Dirac delta function, and (x, y) and (α, β) are the spatial coordinate systems. From this equation we see

that the input signal is carried out by an $(n \times m)$ array of smeared delta functions which are located at

$$\left(n\frac{\lambda}{l}, m\frac{\lambda}{l}\right)$$

in the output plane P_3 . We also note that the intensity of the multiple array of output signals (or images) is proportional to magnitude square of the sinc factors in Eq. (1), i.e.,

$$I_{n, m}(x, y) \propto \left|\text{sinc}\left(n\frac{a}{l}\right)\right|^2 \left|\text{sinc}\left(m\frac{a}{l}\right)\right|^2. \quad (2)$$

Thus the intensity of the higher-order images decreases rapidly as n and m increase. We would, however, treat the zero order (i.e., $m = n = 0$) as the signal and the rest of the diffracted orders as noise. Thus to improve the output SNR, one would make the ratio a/l (where $a \leq l$) approached to unity. However, to make the size of the pixel approach the size of the mesh cell of the device is equivalent to saying that making the x - y drive lines very thin is very difficult to achieve in practice. Nevertheless, if the mesh cell of device l is made smaller and the focal length of transform lens f is made longer, the separation of the output signal with respect to the unwanted noise (i.e., higher-order diffractions) can be obtained. As a numerical example; given $l = 0.127$ mm for a 48×48 -array Light-Mod and $f = 1000$ mm, the mean separation of the output smeared signals would be $\lambda f/l = 4.3$ mm for $\lambda = 5500$ Å. If $l = 0.02$ mm, the mean separation of smeared signals would be ~ 27.5 mm for the same focal length. Thus the input signal size could be as large as 14 mm.

IV. Experimental Results

In our experiments, we show that a piece of 48×48 -array magneto-optics light-mod is used to generate elementary spatial filter in the Fourier plane of a white-light optical processor as depicted in Fig. 3. The pixel size of the device is ~ 0.127 mm, and the size of the light-mod is $\sim 1/4$ in. square. Needless to say that elementary spatial filters can be generated by the device with a programmable computer. Now if we assume a high-pass filter as shown in Fig. 4(a) is being generated in the Fourier plane, an edge-enhanced image can be obtained at the output plane of the processor. Since the magneto-optic device responds to a broad band of light waves (i.e., from red to green), it is, therefore, a simple matter of utilizing the device to generate a color coded high-pass spatial filter. In example, if the polarizer is set at an angle between 95.5 and 104° of Fig. 2, a high-pass color-coded filter of Fig. 4(a) can be generated (i.e., low-pass region is in dark green, while high-pass region is in yellow). And it is apparent that a color-coded edge-enhanced image can be observed at the output plane.

For experimental demonstration, Fig. 4(b) shows a gray scale black-and-white input object. Figure 4(c) is a black-and-white picture of the corresponding color-coded edge-enhanced image obtained with the programmable spatial filter with white-light processing. In the original color image, the edges of the building are

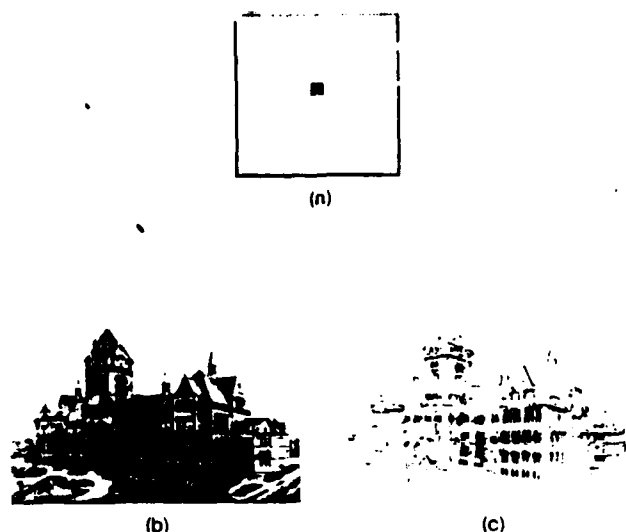


Fig. 4. Edge enhancement: (a) black-and-white picture of a color-coded high-pass filter generated by the device; in reality, the low-pass region is green, and the high-pass region is yellow; (b) input object transparency; (c) black-and-white color-coded edge-enhanced image. In reality, the edges of the building are yellow-white, and the rest of the picture is greenish.

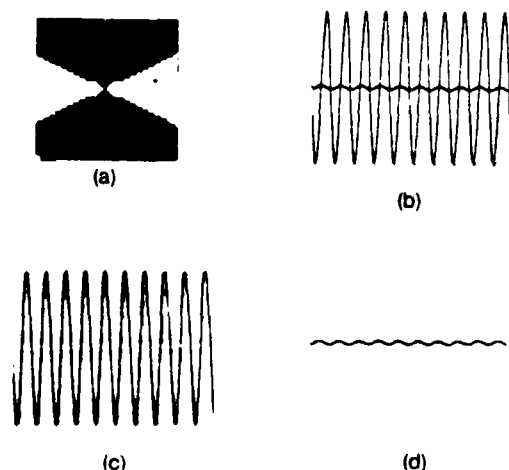


Fig. 5. Directional filtering: (a) black-and-white picture of a wedge filter; (b) input signal; (c) extraction of the larger signal; (d) extraction of the smaller signal.

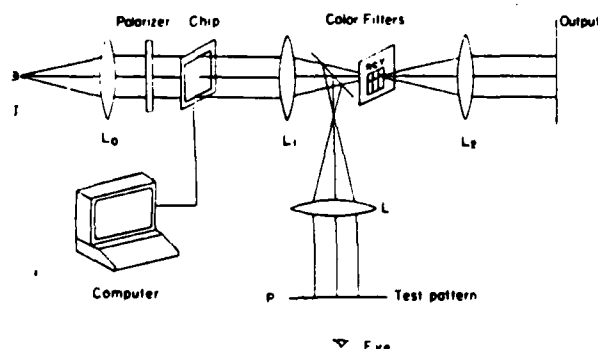


Fig. 6. White-light processor with a programmable input object for pseudocolor encoding: *I*, white-light source; *L*, transform lens.

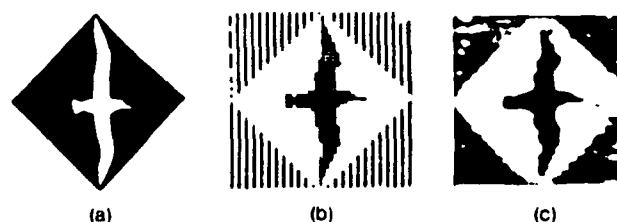


Fig. 7. Pseudocolor encoding: (a) Input object; (b) object pattern generated by the device; (c) a black-and-white color-coded image. In color the bird is yellow, the square region is in green, and the outer region is reddish.

mostly coded in yellow, while the rest of the picture is greenish color. Needless to say that, if the polarizer is set at a different angle, a different shade of color-coded edge-enhanced image can be obtained.

We shall now show a second experimental result obtained with a directional or wedge filter^{6,7} of Fig. 5. Figure 5(a) shows a two-shade radial spectral filter generated by the device. Figure 5(b) shows a black-and-white input object of two sinusoidal waves taken from an oscilloscope. Although these two sinusoidal waveforms are of the same frequency, however, the slopes of these two waveforms are very distinctive. Thus these two sinusoids of different amplitudes can be exclusively extracted with a wedge filter. Figures 5(c) and (d) show a set of the results obtained by the wedge filter of Fig. 5(a), with two sequential settings of the polarizer: Fig. 5(c) is obtained when the vertical region of the wedge filter is coded in black, while the horizontal region is coded in yellow. Figure 5(d) is obtained with a contrast reversed filter of Fig. 5(a).

We shall now demonstrate a theta modulation⁸ pseudocolor encoding technique with this device as shown in Fig. 6. First, a binary black-and-white input object of Fig. 7(a) is placed at the observation plane *P*. Then a pattern of input object can be generated by the Light-Mod with a programmable computer as shown in Fig. 6. The object pattern of the device consists of three distinctive spatially modulated regions as shown in Fig. 7(b). The inner region (i.e., the bird) is modulated with a uniform cross-grating frequency in both directions, while the intermediate region is not modulated, and the outer region is modulated at a lower grating frequency in the horizontal direction. Thus the corresponding smeared object pattern spectra would be spatially separated along the horizontal axis in Fourier plane. In pseudocolor encoding, we allow the zero-order (i.e., the intermediate region) and two first-order (i.e., the bird and the outer region) Fourier spectra to pass through three preselected color filters, (e.g., red, green, and yellow), respectively, at the spatial frequency plane of Fig. 6. Then a pseudocolor-coded image can be obtained at the output plane as shown in a black-and-white picture of Fig. 7(c). Needless to say, different shades of pseudocolor encoded images can also be obtained with different sets of the color filters and different settings of the polarizer orientations. Thus a wide range of pseudocolor images can be obtained with the theta modulation technique.

V. Conclusion

In conclusion, we have incorporated a programmable magneto-optic spatial light modulator with a white light optical signal processor. We have shown that the device responded to polarized white light, in which it offers the advantage of color-coded spatial filters synthesis and the generation of pseudocolor object image. The device can be used as an input programmable object and also as a programmable spatial filter for real-time optical signal processing. Even though the resolution of this device is rather limited, however, we have shown some the interesting applications with the white-light illumination. Nevertheless, one of the important assets of the device must be the programmability, which, in principle, would offer a wide range of real-time processing capabilities. If the resolution of the device is further improved, the device would have significant impact to the application of modern optical signal processing.

We acknowledge the Litton Data Systems for support of the Light-Mod investigation and the support of U.S. Air Force Office of Scientific Research grant AFOSR-83-0140.

References

1. W. E. Ross, D. Psaltis, and R. H. Anderson, "Two-Dimensional Magneto-Optic Spatial Light Modulator for Signal Processing," *Proc. Soc. Photo-Opt. Instrum. Eng.* **341**, 191 (1982).
2. W. E. Ross, D. Psaltis, and R. H. Anderson, "Two-Dimensional Magneto-Optic Spatial Light Modulator for Signal Processing," *Opt. Eng.* **22**, 485 (1983).
3. W. P. Bleha *et al.*, "Application of Liquid Crystal Light Valve to Real Time Optical Data Processing," *Opt. Eng.* **17**, 371 (1978).
4. C. Warde *et al.*, "Microchannel Spatial Light Modulator," *Opt. Lett.* **3**, 196 (1978).
5. F. T. S. Yu, *Optical Information Processing* (Wiley, New York, 1983).
6. F. T. S. Yu, A. Tai, and H. Chen, "Spatial Filtered Pseudocolor Holographic Imaging," *J. Opt.* **9**, 269 (1978).
7. X. J. Lu, "Pseudocolor Encoding with a White-Light Processing System," *Opt. Commun.* **48**, 13 (1983).
8. J. D. Armitage and A. Lohmann, "Theta Modulation in Optics," *Appl. Opt.* **4**, 399 (1965).

SECTION V

Measurement of Noise Performance

Measurement of noise performance for a white-light optical signal processor

Francis T. S. Yu, Le-Nian Zheng, and Fu-Kuo Hsu

A measurement technique for the noise performance of a white-light optical signal processor is presented. The technique utilizes a scanning photometer to trace out the output noise intensity fluctuation of the optical system. The effect of noise performance due to noise perturbation at the input and Fourier planes is measured. The experimental results, except for amplitude noise at the input plane, show the claims for better noise immunity, if the optical system is operating in the partially coherent regime. We have also measured the noise performance due to perturbation along the optical axis of the system. The experimental results show that the resulting output SNR improves considerably by increasing the bandwidth and source size of the illuminator. The optimum noise immunity occurs for phase noise at the input and output planes. For amplitude noise, the optimum SNR occurs at the Fourier plane. In brief, the experimental results confirm the analytical results that we recently evaluated.

I. Introduction

White-light optical processors are known to perform better in noisy conditions compared with coherent optical processors, because the artifact noise in the coherent optical system is unavoidable. The analysis of noise performance under coherent and partial coherent regimes has been quantitatively studied by Chavel and Lowenthal¹ and Chavel.² They show that noise fluctuations caused by the pupil plane can be drastically reduced under broadband illumination. They have also pointed out that the noise at the object plane due to defects other than the phase deviations cannot be suppressed under partially coherent illumination.

Recently, Leith and Roth³ studied the noise performance of an achromatic coherent optical processor. They demonstrated that such a system shows considerable noise immunity if a broad spectral band source is employed. More recently, we analyzed the performance of a white-light optical processor under noisy environment.^{4,5}

We have shown that except for the case when the amplitude noise is present at the input plane, the resulting output SNR improves considerably by in-

creasing the number of filter channels (or equivalently the spectral bandwidth) and the size of the light source employed.

In this paper, we shall experimentally measure the noise performance of a white-light optical processor. We shall show that the measured results confirm the analytical predictions.^{4,5} Aside from the noise effects at the input and Fourier planes, we have also measured the noise performance due to thin noise effects along the longitudinal direction (i.e., Z axis) of a white-light optical system.

II. Noise Measurement

The white-light optical signal processor to be studied here is described in Fig. 1. The processor is similar to that of a coherent optical processor, except for the use of an extended white-light source, source encoding mask, sampling phase grating, and achromatic Fourier transform lenses. The output light intensity distribution due to the n th narrow spectral band spatial filter in the Fourier plane can be determined by the following integral equation⁴⁻⁶:

$$I(x', y') = \int_{\lambda_{ln}}^{\lambda_{hn}} \iint \gamma(x_0, y_0) \cdot \left| \iint S(x_0 + \alpha - \lambda/\nu_0, y_0 + \beta) H_n(\alpha, \beta) \cdot \exp \left[-i \frac{2\pi}{\lambda f} (x' \alpha + y' \beta) \right] d\alpha d\beta \right|^2 dx_0 dy_0 d\lambda, \quad (1)$$

where $\gamma(x_0, y_0)$ represents the intensity distribution of the light source at P_0 , λ_{hn} and λ_{ln} are the longest and shortest limiting wavelengths of the n th spectral band filter $H_n(\alpha, \beta)$, $S(x_0 + \alpha - \lambda/\nu_0, y_0 + \beta)$ is the smeared

The authors are with Pennsylvania State University, Electrical Engineering Department, University Park, Pennsylvania 16802.

Received 3 July 1984.

0003-6935/85/020173-06\$02.00/0.

© 1985 Optical Society of America.

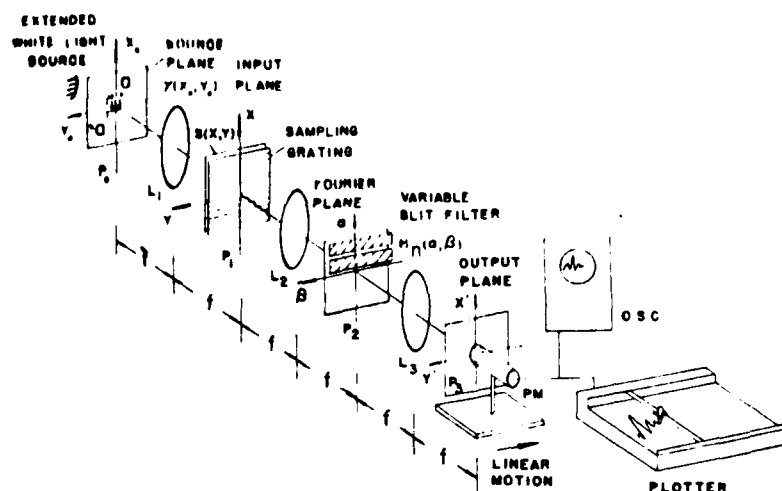


Fig. 1. Grating-based white-light optical processor: $\gamma(x_0, y_0)$, source intensity distributions; P_0 , source plane; P_1 , input plane; P_2 , Fourier plane; P_3 , output plane; $s(x, y)$, object transparency; $H_n(\alpha, \beta)$, slit filter; PM , photometer; OSC , oscilloscope; L , achromatic transform lenses.

Fourier spectra of the input object $s(x, y)$, $H_n(\alpha, \beta)$ is the n th spectral band spatial filter corresponding to the n th channel in the system, f is the focal length of the achromatic Fourier transform lens, and ν_0 is the spatial frequency of the sampling phase grating, which can be written as

$$T(x) = \exp(i2\pi\nu_0 x). \quad (2)$$

We shall first investigate the noise performance of the proposed white-light processor under the spatially coherent illumination, i.e., the effects due to source size. For convenience, we assume that the source irradiance is uniform over a square aperture at source plane P_0 , which can be written as

$$\gamma(x_0, y_0) = \text{rect}\left(\frac{x_0}{a}\right) \text{rect}\left(\frac{y_0}{a}\right), \quad (3)$$

where

$$\text{rect}\left(\frac{x_0}{a}\right) \triangleq \begin{cases} 1, & |x_0| \leq \frac{a}{2} \\ 0, & |x_0| > \frac{a}{2} \end{cases}$$

For simplicity, we assume that the input signal is a 1-D object independent of the y axis. The Fourier spectrum would also be 1-D in the β axis but smeared into rainbow colors along the α direction. Let the width of the n th narrow spectral band filter be $\Delta\alpha_n$. If the filter is placed in the smeared Fourier spectra, the spectral bandwidth of the filter can be written as

$$\Delta\lambda_n = \lambda_{hn} - \lambda_{ln} \approx \frac{\Delta\alpha_n}{\nu_0 f}. \quad (4)$$

The total number of filter channels can be determined,

$$N \triangleq \frac{\Delta\lambda}{\Delta\lambda_n} \approx \frac{\Delta\lambda \nu_0 f}{\Delta\alpha_n}, \quad (5)$$

where $\Delta\lambda$ is the spectral bandwidth of the white-light source. Thus, we see that the degree of temporal coherence at the Fourier plane increases as spatial frequency of the sampling grating ν_0 increases.

For the noise measurement under temporally coherent illumination, we would use a variable slit representing a broad spectral filter in the Fourier plane. The output noise fluctuation can be traced out with a linearly scanned photometer, as illustrated in Fig. 1. It is therefore apparent that the output noise fluctuation due to spectral bandwidth of the slit filter and due to the source size can then be separately determined. We shall adopt the definition of output signal-to-noise ratio (SNR), as proposed in a previous paper,⁴ for the measurement of the noise performance, i.e.,

$$\text{SNR}_n(y') \triangleq E[I_n(y')]/\sigma_n(y'), \quad (6)$$

where $I_n(y')$ is the output irradiance due to the n th channel, $E[\cdot]$ denotes the ensemble average, and $\sigma_n^2(y')$ is the variance of the output noise fluctuation, i.e.,

$$\sigma_n^2(y') \triangleq E[I_n^2(y')] - [E[I_n(y')]]^2. \quad (7)$$

Evidently the output intensity fluctuation $I_n(y')$ can be traced out by a linearly scanned photometer. The dc component of the output traces is obviously the output signal irradiance (i.e., $E[I_n]$), and the mean square fluctuation of the traces is the variance of the output noise (i.e., σ_n^2). Thus we see that the effect of the output SNR due to spectral bandwidth (i.e., temporal coherence) and source size (i.e., spatial coherence) can readily be obtained with the proposed measurement technique.

III. Experimental Results

In our experiments, a 75-W xenon arc lamp is used as the white-light source. The spatial frequency of the sampling phase grating used is ~ 50 lines/mm, the focal length of the achromatic transform lenses is ~ 380 mm. Both the amplitude and the phase noise plates used in the experiments are generated by photographing a laser speckle pattern, and the phase plate is obtained with a surface relieving technique through an R-10 bleaching process.⁷ Shower glass, for strong phase perturbation, is also utilized in the experiments. We shall first demonstrate the noise performance due to perturbation



Fig. 2. Effect on output image (with a section of photometer traces) due to phase noise at the input plane for different spectral bandwidths. The source size used is 0.7 mm square (i.e., $a = 0.7$ mm): (a) $\Delta\lambda_n = 1500$ Å; (b) $\Delta\lambda_n = 1000$ Å; (c) $\Delta\lambda_n = 500$ Å.

at the input plane. For the amplitude noise at the input plane, the experiments have shown that there is no apparent improvement in noise performance under partially coherent illumination. The result is quite conclusive with the previous prediction.^{3,4} However for the phase noise at the input plane, the noise performance of the system is largely improved with a partially coherent illumination. We shall first utilize a weak phase model (obtained by laser speckle and a photographic bleaching process described earlier) as the input noise. Now we consider the situation of an input object transparency superimposing with the phase noise at the input plane. The effect of the noise performance of the optical system can then be obtained by varying the source size and the spectral bandwidth of the slit filter, as described in Fig. 1. Figure 2 shows a set of output photographic images together with sections of corresponding photometer traces to illustrate the effect due to spectral bandwidth of the slit filter. From these pictures we see that the noise performance (i.e., SNR) improves as the spectral bandwidth (i.e., temporal coherence) of the slit filter increases.

Quantitative measurements of the noise performance due to phase noise at the input plane are plotted in Figs. 3 and 4. From these two figures we see that the output SNR increases monotonically as the spectral bandwidth $\Delta\lambda_n$ of the slit filter increases and it linearly increases as the source size enlarges. Thus the noise performance for a partially coherent optical system improves as the degree of coherence (i.e., temporal and spatial coherence) relaxes. In other words, to improve the output SNR of the white-light (i.e., partially coherent) processor, one can either relax the spatial coherence (i.e., the source size) or the temporal coherence (i.e., the spectral bandwidth of the filter) or both in the optical processing system. We stress that the experimental results are quite compatible with the results obtained in our recent analysis.^{4,5}

Let us now demonstrate the effect of the noise performance due to strong phase noise. In the experiments, a conventional shower glass is used as the input phase noise. Figure 5 shows a set of results we obtained

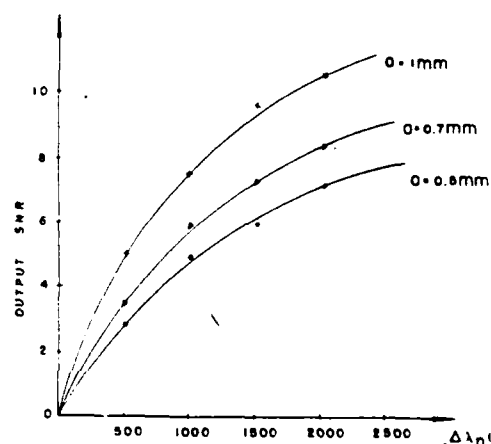


Fig. 3. Output SNR for phase noise at the input plane as a function of spectral bandwidth of the slit filter for various values of source sizes.

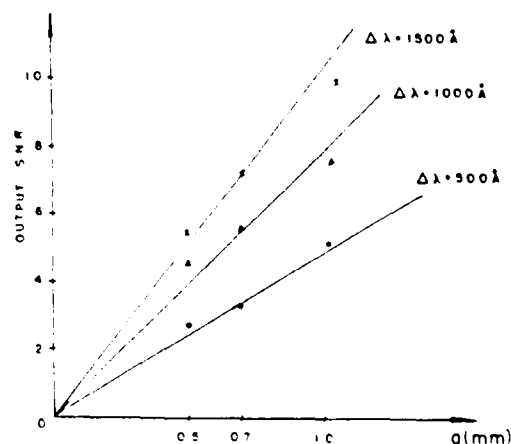


Fig. 4. Output SNR for phase noise at the input plane as a function of source size for various values of spectral bandwidths.

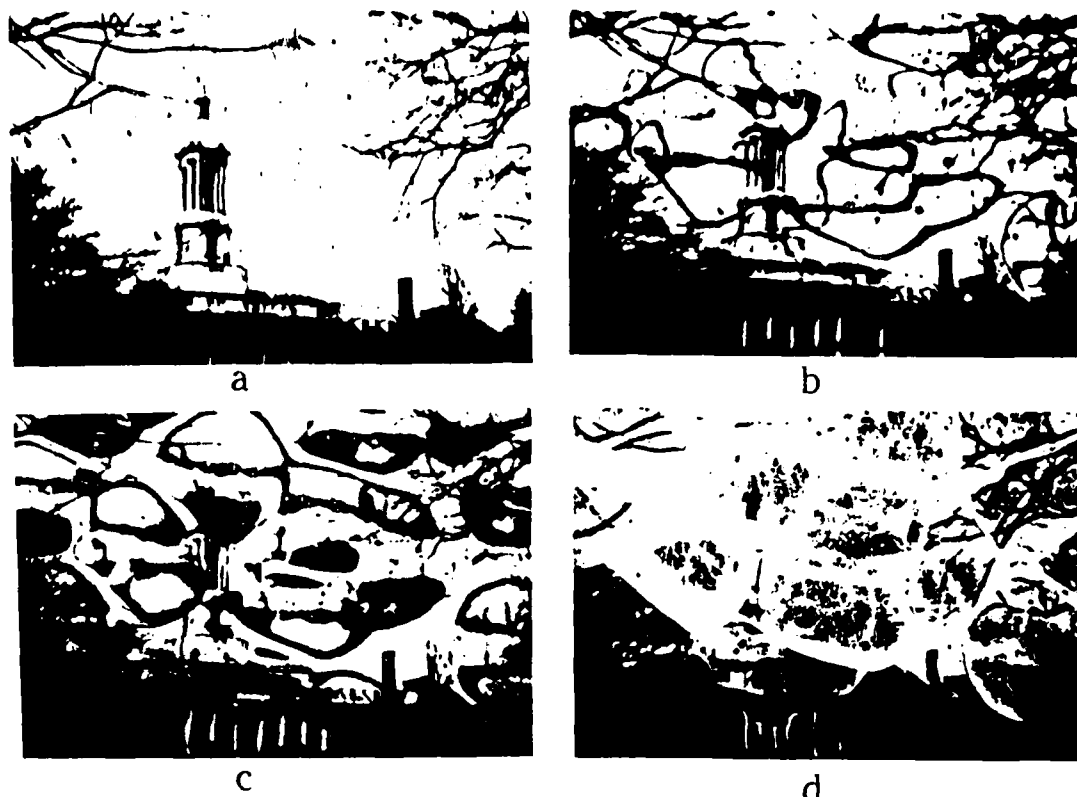


Fig. 5. Effect of output image due to strong phase perturbation at the input plane ($a = 0.7$ mm): (a) $\Delta\lambda_n = 3000$ Å; (b) $\Delta\lambda_n = 1500$ Å; (c) $\Delta\lambda_n = 500$ Å; (d) obtained with a He-Ne laser.

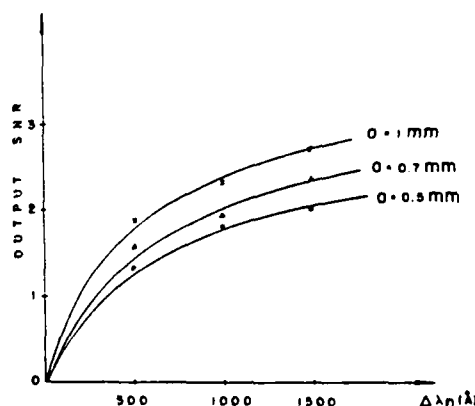


Fig. 6. Output SNR for amplitude noise at the Fourier plane as a function of spectral bandwidth for various source sizes.

under various spectral bandwidth illuminations. Figure 5(a) shows an output result obtained under entire broadband white-light illumination. Although this image is somewhat aberrated due to the thick phase perturbation, the image is relatively immune from random noise fluctuation. Compared with the results obtained from Figs. 5(a)–(d), we see that the output SNR decreases rather rapidly as the spectral bandwidth of the slit filter decreases. Furthermore, Fig. 5(d) shows a result obtained with a narrowband coherent source (i.e., a He-Ne laser). Aside from the poor noise per-

formance, we have noted that the output image is also severely corrupted by coherent artifact noise.

We shall now demonstrate the noise performance of a white-light optical processing system due to noise at the Fourier plane. With reference to the same measurement technique as proposed in Fig. 1, the effects of amplitude noise at the Fourier plane are plotted in Fig. 6. In contrast with the amplitude noise at the input plane, we see that the output SNR increases monotonically as the spectral bandwidth of the slit filter increases. The output SNR also improves as the source size enlarges. Thus, for amplitude noise at the Fourier plane, the noise performance of a white-light optical processor improves as the degree of temporal and spatial coherence decreases.

Figure 7 shows the noise performance of a white-light processor for phase noise at the Fourier plane. From this figure, once again we see that the output SNR is a monotonic increasing function of spectral bandwidth $\Delta\lambda_n$. The SNR also increases as the source size increases. However, compared with the case of phase noise at the input plane of Fig. 2, the improvement of the noise performance is somewhat less effective compared with the phase noise at the input plane. Once again we see that the experimental results are compatible with the analytical results that we obtained in our previous papers.^{4,5}

We shall now provide the result of noise performance due to thin phase noise along the optical axis (i.e., Z

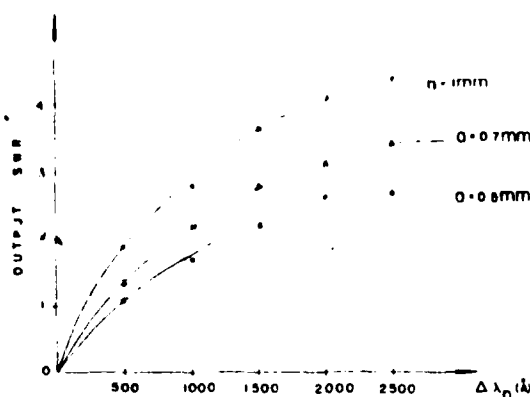


Fig. 7. Output SNR for phase noise at the Fourier plane as a function of source size for various values of spectral bandwidths.

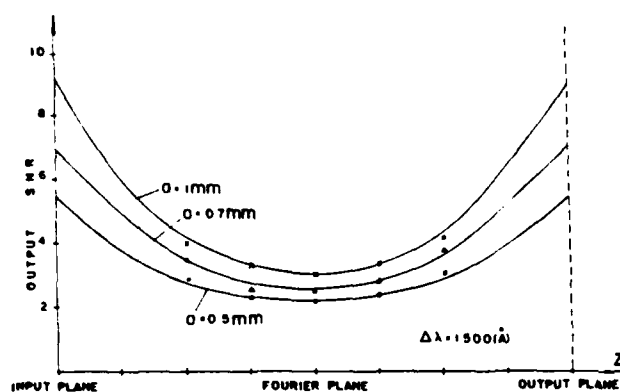


Fig. 8. Variation of the output SNR due to thin phase noise as a function of the Z direction for various source sizes.

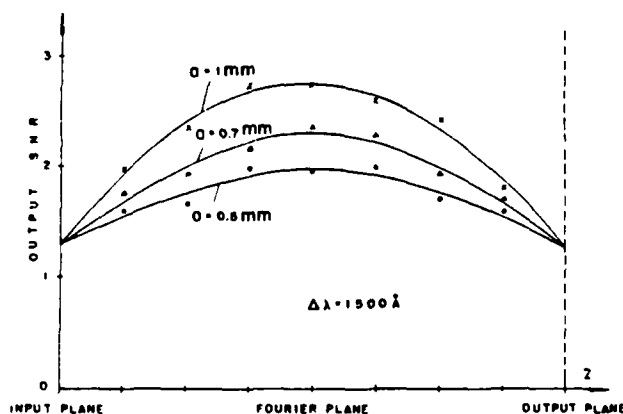


Fig. 9. Variation of the output SNR due to thin amplitude noise as a function of the Z direction for various source sizes.

axis) of the optical system. Figure 8 shows the variation of output SNR due to phase noise inserted in various planes of the optical system. From this figure we see that the output SNR improves drastically for phase noise inserted at the input and output planes under temporal and spatial partially coherent illumination. The noise performance is somewhat less effective for the phase noise at the Fourier plane, even under partially

coherent illumination. Nonetheless, the phase noise at the Fourier plane can, in principle, be totally eliminated under very broadband illumination, if each of the noise channels is uncorrelated. We have also noted that the output SNR is somewhat lower for higher spatial coherent illumination (i.e., smaller source size). In other words, the output SNR can also be improved with extended source illumination.

The noise performance, due to amplitude noise along the Z axis of the proposed optical processor, is plotted in Fig. 9. From this figure we see that the output SNR improves as the noise perturbation moved away from the input and output planes and where the optimum SNR occurs at the Fourier plane. Again, we see that the output SNR is somewhat higher for larger source sizes (i.e., lower degree of spatial coherence). However we stress that the noise performance cannot be improved with partially coherent illumination, if the amplitude noise is placed at the input or at the output plane.

IV. Summary and Conclusion

We have devised a technique for measuring the noise performance of a white-light (i.e., partially coherent) optical signal processor. We have utilized a scanning photometer method to obtain the output intensity traces of a partially coherent system operating in noisy conditions. The effects of output SNR due to the amplitude and the phase noise at the input and Fourier planes were quantitatively studied. The experimental results show that there has been no improvement in noise performance due to amplitude noise at the input plane. However the output SNR improves drastically for the phase noise at the input plane with a partially coherent (i.e., temporal and spatial coherence) illumination. For very strong input phase disturbance, the experiments show that the output noise can essentially be eliminated, if it is under very broadband illumination.

As for the performance due to noise at the Fourier plane, the experimental results show that the output SNR improves for both the amplitude and phase noise under a partially coherent regime. However the overall improvement is somewhat lower than the effect due to phase noise at the input plane, under the same partially coherent (i.e., temporal and spatial coherence) illumination.

We have also measured the noise performance due to thin noise effects along the Z axis of the optical processing system. The experimental results show that optimum noise immunity occurs for phase noise at the input and output planes, and optimum output SNR occurs for amplitude noise at the Fourier plane. The results also indicate that a higher output SNR can in fact be obtained for more relaxed temporal and spatial coherence constraints.

In concluding this paper we stress that the experimental results are quite compatible with the analytical results that we recently evaluated.^{4,5}

We acknowledge the support of the U.S. Air Force Office of Scientific Research grant AFOSR-83-1040.

References

1. P. Chavel and S. Lowenthal, "Noise and Coherence in Optical Image Processing. II: Noise Fluctuations," *J. Opt. Soc. Am.* **68**, 721 (1978).
2. P. Chavel, "Optical Noise and Temporal Coherence," *J. Opt. Soc. Am.* **70**, 935 (1980).
3. E. N. Leith and J. A. Roth, "Noise Performance of an Achromatic Coherent Optical System," *Appl. Opt.* **18**, 2803 (1979).
4. F. T. S. Yu, K. S. Shaik, and S. L. Zhuang, "Noise Performance of a White-Light Optical Signal Processor. I: Temporally Partially Coherent Illumination," *J. Opt. Soc. Am. A* **1**, 489 (1984).
5. F. T. S. Yu, K. S. Shaik, and S. L. Zhuang, "Noise Performance of a White-Light Optical Signal Processor. II: Spatially Partially Coherent Illumination," *Appl. Phys.* **B36**, 1 (1985).
6. M. Born and E. Wolf, *Principles of Optics* (Pergamon, New York, 1964).
7. B. J. Chang and K. Winick, "Silver-Halide Gelatin Holograms," *Proc. Soc. Photo-Opt. Instrum. Eng.* **215**, 172 (1980).

SECTION VI

White-Light Fourier Holography

WHITE-LIGHT FOURIER HOLOGRAPHY

F.T.S. YU and F.K. HSU

*Electrical Engineering Department, The Pennsylvania State University,
University Park, PA 16802, USA*

Received 17 August 1984

This paper describes a technique for generating broad spectral band Fourier holograms with an encoded white light source. Since this technique utilizes primary white-light construction and reconstruction process, it is quite suitable for color Fourier hologram image reconstruction. Experimental results are also given.

1. Introduction

The construction of Fourier transform hologram for a two-dimensional object transparency with coherent optics was first introduced by Vander Lugt in 1964 in the application to complex signal detection [1]. Since then efforts have been made to develop techniques for making Fourier holograms with incoherent light.

Recently, Courjon and Bulabois [2-4] had demonstrated a technique of producing Fourier holograms with a spatially incoherent source. They utilized an interference filter and a holographic transparency to achieve a high degree of coherence illumination for the Fourier hologram construction and the hologram image reconstruction was obtained with narrow spectral band illumination. Although good experimental results have been reported, however the technique is limited to monochrome hologram image reconstruction. Ferriere et al. [5] have also demonstrated a technique of generating Fourier holograms with an incoherent source. They utilized dispersive prisms and a slit filter to achieve a high temporal coherence (i.e., narrow band illumination) for Fourier hologram generation. Although positive results have been reported in their article, however the image quality is rather poor. The major drawback of this technique must be due to low-light construction process, in which results with poor noise performance.

In this paper we shall describe a technique of pro-

ducing a broad band Fourier hologram with a white-light source. The technique utilizes a high efficient dispersive grating and a source encoding mask for the Fourier hologram generation. Since the hologram construction utilizes all colors of visible light, this technique is suitable for color Fourier hologram image reconstruction.

2. Construction and reconstruction process

We shall now describe a technique of generating a broad spectral band Fourier hologram with a white-light processing technique [6], as schematized in fig. 1. A high diffraction efficient phase grating is used to disperse the spectral content of the light source into rainbow color at the back focal plane of the achromatic lens L_0 . To alleviate the constraint of recording medium due to limited dynamic range, we shall spatially sample the smeared optical light source with periodic pinholes such that a sequence of partially coherent sources for various spectral colors can be obtained at the source plane P_0 . The intensity distribution of these encoded sources, for various λ_n , would be

$$\gamma(x_0, y_0) = K \sum_{n=1}^N \text{cir}_n [|x_0, y_0 - f_0 \lambda_n| / \Delta \gamma_n], \quad (1)$$

where K is a proportionality constant,

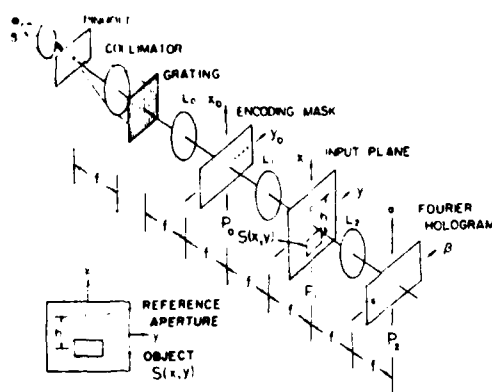


Fig. 1. A technique of generating a broad spectral band Fourier hologram with a white-light source. S, white-light source.

$$\text{cir}_n[r/\Delta r_n] \doteq 1, \quad 0 \leq r \leq \Delta r_n, \\ \doteq 0, \quad \text{otherwise,}$$

Δr_n is the radius of the n th sampling pinholes, f is the focal length of the achromatic lens, ν_0 is the spatial frequency of the phase grating, λ_n is the main wavelength within the n th sampled source, and (x_0, y_0) is the spatial coordinate system of the source plane P_0 . To achieve the required spatial coherence at the input plane P_1 , it is apparent that the size of the sampling pinholes should be small compared with the overall input object, such as

$$\Delta r_n < f\lambda_n/h. \quad (2)$$

where h denotes the separation between the reference point and the input object $s(x, y)$ as shown in fig. 1.

To maintain a high temporal coherence for Fourier hologram construction, it is required that the wavelength spread $\Delta\lambda_n$ over the n th sampling aperture should satisfy the following inequality

$$\Delta\lambda_n/\lambda_n \ll \Delta\nu/\nu_0, \quad (3)$$

where $\Delta\nu$ is the spatial frequency bandwidth of the input object $s(x, y)$ and ν_0 is the spatial frequency of the phase grating.

Thus we see that a sequence of encoded partially coherent sources are illuminating the input plane P_1 . Since the source encoding mask is covered over a wide spectral content of the smeared white-light source, it is apparent that N discrete Fourier holograms, for dif-

ferent wavelengths, can be synthesized. Let us now assume that the input plane contains an object transparency and a reference pinhole, as described in the following equation:

$$f(x, y) = s(x + h/2, y) + \delta(x - h/2, y), \quad (4)$$

where $s(x, y)$ denotes an input object function, $\delta(x, y)$ denotes the Dirac delta function, and h is the main separation between the target and the reference pinholes. It is therefore apparent that a broad band Fourier hologram can be interferometrically generated in the Fourier plane P_2 . If we assume that the holographic construction is in the linear region of the recording emulsion, the amplitude transmittance distribution of the recorded Fourier hologram would be

$$H(\alpha, \beta) \approx \sum_{n=-N}^N \{K_1 |S(\alpha, \beta + f\nu_0\lambda_n)|^2 \\ + K_2 |S(\alpha, \beta + f\nu_0\lambda_n)| \\ \times \cos[(2\pi h/\lambda_n f)\alpha + \phi(\alpha, \beta + f\nu_0\lambda_n)]\}, \quad (5)$$

where K_1 and K_2 are arbitrarily proportional constants, $S(\alpha, \beta; \lambda_n)$ is the Fourier spectrum of input object function $s(x, y; \lambda_n)$, (α, β) is the spatial coordinate system of the Fourier plane, λ_n is the main wavelength of the n th quasi monochromatic coherent source, f is the focal length of the achromatic transform lens L_2 , and ν_0 is the spatial frequency of the grating.

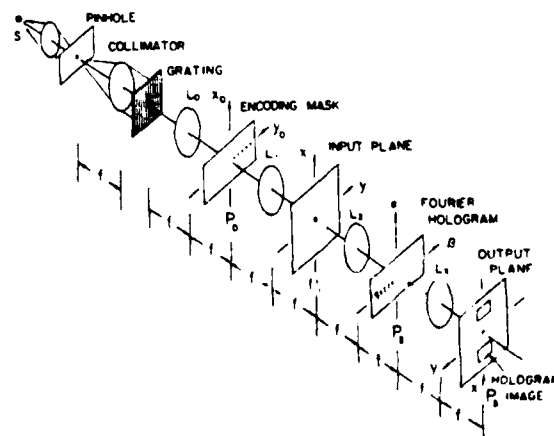


Fig. 2. Fourier hologram image reconstruction with white-light processing.

It is interesting to note that if the broad band hologram $H(\alpha, \beta)$ is illuminated by a beam of encoded white-light source (shown in fig. 2) such as

$$E(\alpha, \beta; \lambda) = C \sum_{n=-N}^N \text{cir}_n(\alpha, \beta + f\nu_0\lambda_n; \lambda), \quad (6)$$

where C is a complex proportionality constant, then the complex light field at the output plane would be

$$g(x, y; \lambda) = \iint E(\alpha, \beta; \lambda) H(\alpha, \beta) \times \exp[-i(2\pi/\lambda f)(\alpha x + \beta y)] d\alpha d\beta. \quad (7)$$

By substituting eqs. (5) and (6) into eq. (7), we have

$$g(x, y; \lambda) = \sum_{n=1}^N C_1 \delta(x, y; \lambda) * s(x, y; \lambda_n) * s^*(-x, -y; \lambda_n) + \sum_{n=1}^N C_2 \delta(x, y; \lambda) * [s(x+h, y; \lambda_n) + s^*(-x+h, -y; \lambda_n)], \quad (8)$$

where C_1 and C_2 are complex constants, $*$ denotes the convolution operation and the superscript $*$ represents the complex conjugation. The corresponding output irradiance can be shown as

$$I(x, y) = \int_{\Delta\lambda_n} |g(x, y; \lambda)|^2 d\lambda, \quad \text{for } n = 1, 2, \dots, N, \quad (9)$$

which is approximated by

$$I(x, y) \approx \Delta\lambda_n \sum_{n=1}^N \{K_1 s(x, y; \lambda_n) * s^*(x, y; \lambda_n) + K_2 [|s(x+h, y; \lambda_n)|^2 + |s(x-h, y; \lambda_n)|^2]\}, \quad (10)$$

where K_1 and K_2 are proportionality constants, $*$ denotes the correlation operation. From this equation we see that two hologram images of $s(x, y)$ would be diffracted around $x = \pm h$ at the output image plane of fig. 2.

3. Experimental result

We would now provide a couple of experimental results obtained with the proposed white-light Fourier holographic process. In our experiments, a 75-W xenon arc lamp with a 1 mm square pinhole is used as a white-light source. A sinusoidal phase grating of about 110 lines/mm, with 25% diffraction efficiency for the first-order diffraction, is used to disperse the spectral content of the light source. The achromatic transform lenses used are about 750 cm focal length. The source encoding mask composes a set of periodic circular pinholes of about 40 μm and their spacing is about 2.5 mm. The separation between the reference aperture and the input target object is about 8 mm. The size of the reference aperture is roughly about 300 μm .

We shall now show a couple of Fourier hologram images obtained with this white-light processing technique. Fig. 3(a) shows a gray scale object, with a reference pinhole, used as an input transparency. A broad-band Fourier hologram is generated as shown in the enlarged photograph of fig. 3(b). Fig. 3(c) shows a pair of twine holographic images obtained with this technique. As compared with the original object, the feature of the hologram image can readily be seen, although the image quality is still needed to improve.

One of the features of the white-light Fourier holography must be the color image reconstruction. Fig. 4(a) shows a set of binary color English characters, with a reference pinhole, used as input object to generate a broad-band color Fourier hologram. Fig. 4(b) shows a pair of color holographic images obtained with this technique. Although the image quality of this result is still somewhat poor, however as compared with the original transparency, the color reproduction is rather faithful. Nevertheless, this result may be the first white-light colour Fourier hologram image that is ever reconstructed.

4. Conclusion

We have described a technique of generating a broad spectral band (i.e., white-light) Fourier hologram. The technique utilizes light dispersion and source sampling method to obtain a set of narrow-band partially coherent sources for the hologram construction process. Since the technique utilizes

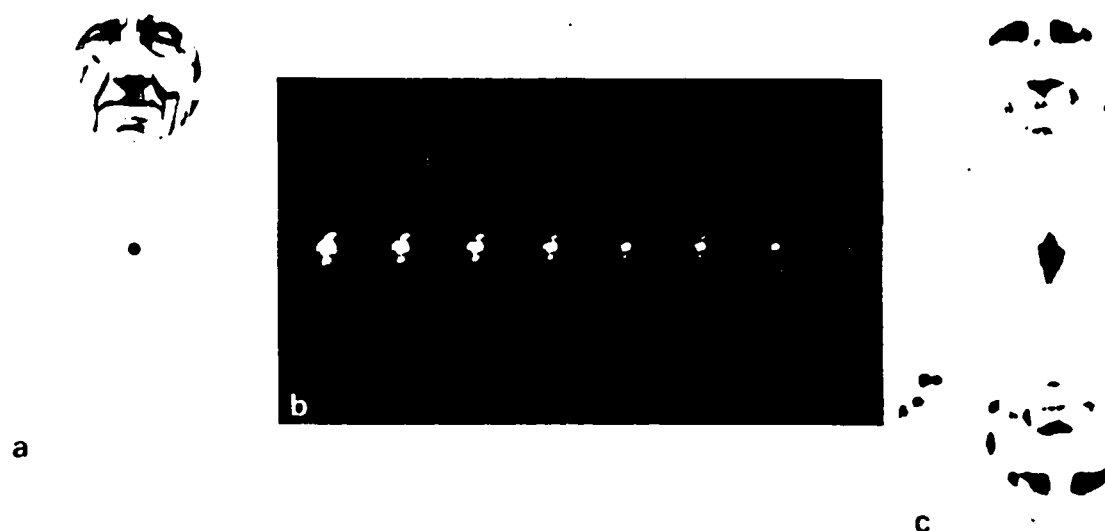


Fig. 3. Fourier hologram image reconstruction. (a) Input object with a reference pinhole. (b) A broad band Fourier hologram. (c) Fourier hologram images.

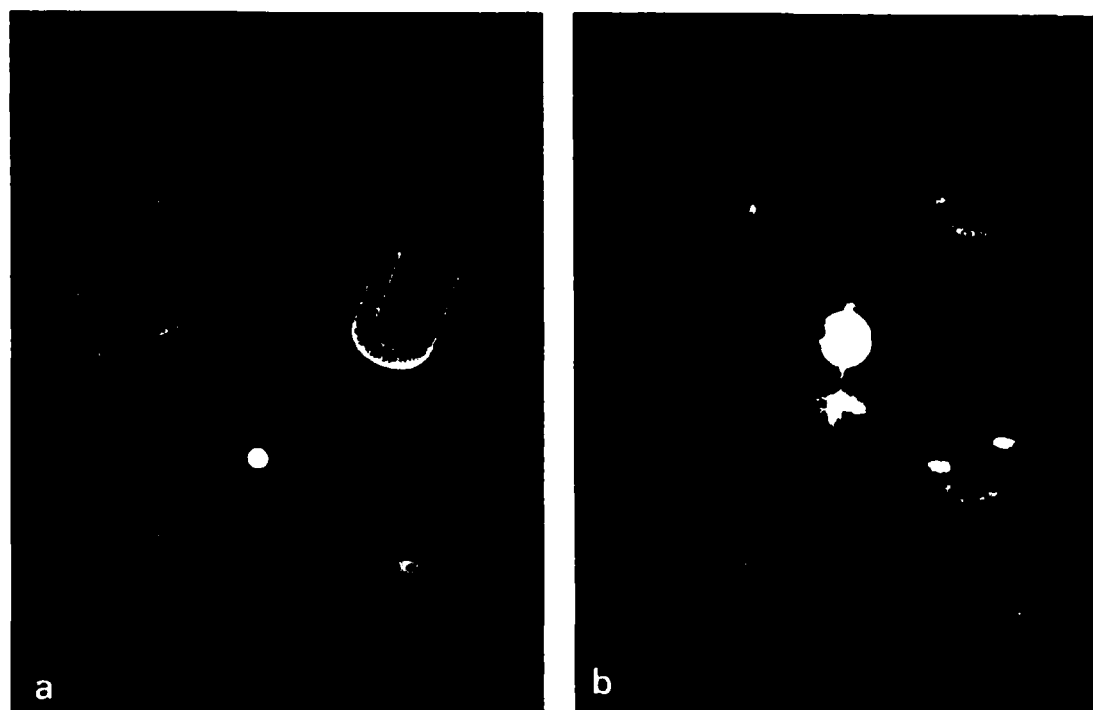


Fig. 4. Color hologram image. (a) Input object with reference pinhole. (b) Color Fourier hologram images.

white-light illumination, it is quite suitable for color Fourier holographic imaging.

Acknowledgement

We acknowledge the support of the U.S. Air Force Office of Scientific Research AFOSR Grant 83-0140.

References

- [1] A. Vander Lugt, *IEEE Trans. Inform. Theory* **11-10** (1964) 139.
- [2] D. Courjon and J. Bulabois, *Optics Comm.* **21** (1977) 96.
- [3] D. Courjon and J. Bulabois, *Optics Comm.* **31** (1979) 270.
- [4] D. Courjon and J. Bulabois, *SPIE* **194** (1979) 129.
- [5] R. Ferriere, J.P. Goedgebuer and J.C. Vienot, *Optics Comm.* **31** (1979) 285.
- [6] F.T.S. Yu, *Optical information processing* (Wiley-Interscience, New York, 1983).

SECTION VII

Optical Generation of Speech Spectrogram

White-light optical speech spectrogram generation

F. T. S. Yu, T. W. Lin, and K. B. Xu

A white-light optical processing technique of generating speech spectrogram is presented. The speech spectrograms thus generated are frequency color-coded resulting in easier visual discrimination. The temporal-to-spatial conversion of speech signal is accomplished by means of density modulation with a CRT scanner. The scaling procedure of the speech spectrogram as well as the frequency resolution limit of the system is discussed. Experimental demonstrations of the proposed frequency color coded speech spectrograms generated by the proposed white-light optical processing technique are given.

I. Introduction

Since development of the first electronic sound spectrograph by Bell Telephone Laboratories nearly four decades ago,¹ great strides have been made in the field of speech analysis. The electronically generated sound spectrograph has been widely used for various applications including such areas as linguistics, phonetics, speech synthesis, and speech recognition. However, an optical system utilizing the Fourier transform properties of the positive lens offers a viable alternative to the electronic counterpart. The multichannel optical processor suggested by Cutrona *et al.*² was found to be able to utilize efficiently the 2-D nature of an optical system. Moreover, by sacrificing the multichannel capability of such a processor, Thomas³ pointed out the feasibility of generating a near real time spectrum analysis for large space-bandwidth signal. Later Yu⁴ reinforced Thomas's concept in the synthesis of a coherent optical sound spectrograph. He pointed out that a near real time optical sound spectrograph can be designed and constructed at a competitively low cost.⁵

In this paper, we will describe a technique of generating multicolor speech spectrograms with a white-light optical processor. This technique utilizes a cathode ray tube (CRT) scanner density modulator to convert a temporal signal to a spatial signal that is suitable for white-light signal processing. To obtain a color-coded speech spectrogram, a dispersive element such as a

grating (or prism) can be used at the input plane of the processor. In frequency color encoding, a narrow slit is placed over the smeared color signal spectra at the Fourier plane so that a frequency color encoded spectrogram can be recorded. In the following, we shall describe the basic performance of this white-light optical spectrum analyzer as applied to speech signals. The frequency resolution limit of the system as well as the frequency scaling of the spectrogram will be given. Experimental demonstrations of the color-coded speech spectrograms, obtained with the white-light processing technique, will be provided.

II. Temporal-Spatial Signal Conversion

It is well known that an optical processor is capable of performing 2-D spatial Fourier transformation. However, the processing of time signals by optical means necessitates the transformation of the signals to a 2-D spatial format. Generally speaking, there are two ways of performing this conversion, namely, the density and the area modulation techniques.⁶ Nevertheless, the density modulation method is the simplest and most commonly used technique in practice.⁷ We shall use a density modulation technique for temporal-to-spatial signal conversion and also show that the temporal-spatial formats obtained from this technique are very suitable for color-coded spectrogram generation with a white-light source.

The conversion can be obtained by displaying the time signal with a CRT scanner and then recorded on a moving photographic film. In other words, the time signal is first applied to the Z axis of a high-resolution CRT scanner to produce an intensity modulated electron beam so that the fluorescence light intensity varies linearly with the input signal voltage. Since the signal voltage is usually a bipolar function and the light intensity is a positive real quantity, an appropriate bias should be added with the time signal to produce a density modulated signal. To ensure a linear density

The authors are with Pennsylvania State University, Electrical Engineering Department, University Park, Pennsylvania.

Received 10 September 1984.

0003-6935/85/060836-06\$02.00/0.

© 1985 Optical Society of America.

modulated signal, the input signal should be scaled down within the linear region of the CRT scanner. Furthermore, a ramp function is fed into the Y axis of the CRT scanner to produce the vertical sweep. To maintain the uniformity of sweep intensity, the scan rate should be set considerably higher than the maximum frequency content of the input signal. Thus the signal would be displayed on the CRT screen as a uniform intensity scan at each vertical sweep. Consequently, a spatially recorded format, whose amplitude transmittance is linearly proportional to the intensity of CRT display, can be produced by imaging the CRT display onto a moving photographic film. Figure 1(a) shows the schematic diagram of the conversion process. The recorded format, as typified in Fig. 1(b), can then be inserted into the input plane of the optical processor for spectrogram generation.

In the time-spatial conversion recording, the speed of the recording film limits the highest-frequency content of the signal to be recorded. For example, if the highest frequency content of the signal is ν cps, the speed of the film motion should be

$$v \geq \nu/R, \quad (1)$$

where R is the spatial frequency limit of the film. Thus it is apparent that to resolve the highest frequency content of the recorded format, the speed of the recording film should be so adjusted higher than the ratio of ν/R . Unfortunately, the finite optical processing window would set the speed limit of the recording film. A higher speed of the recording film would result in a lower frequency resolution of the spectrogram generation, thus corresponding to a wideband spectrogram analysis.⁸ However, this drawback may be alleviated by utilizing a higher-resolution CRT scanner. Nevertheless, in practice, a higher-resolution CRT tends to be more expensive. Moreover, the frequency resolution of the optical processor is also limited by the source size as well as the point spread function of the imaging lens and, of course, the width of the optical window in the processor. Thus the speed of recording film should be restricted by the following inequality:

$$v \leq W\nu_l, \quad (2)$$

where W is the width of the optical window of the processor and ν_l is the lowest frequency limit.

III. System Analysis

Let us now discuss a white-light optical spectrum analyzer as depicted in Fig. 2, where L_1 , L_2 , and L_3 are achromatic Fourier transform lenses. If the recorded format of a time-spatial signal, as described in Sec. II, is loaded in a linear motion film transport at the input plane of the processor, a slanted set of rainbow smeared Fourier spectra in the Fourier plane can be observed. We note that the effect of the phase grating at the input plane is to disperse the signal spectra in a direction perpendicular to the recorded input format (i.e., direction of the film motion), so that a set of nonoverlapping slanted (or fan-shaped) rainbow color smear spectra can be displayed at the Fourier plane. It is now

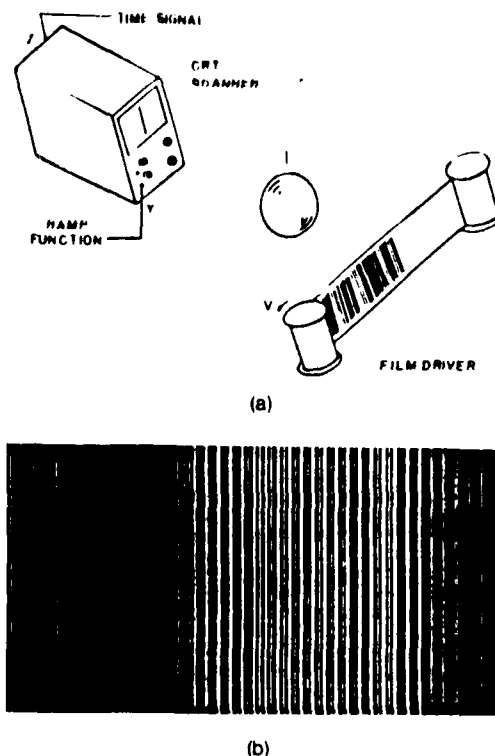


Fig. 1. (a) Temporal-to-spatial signal conversion. L , imaging lens. (b) Segment of recorded format.

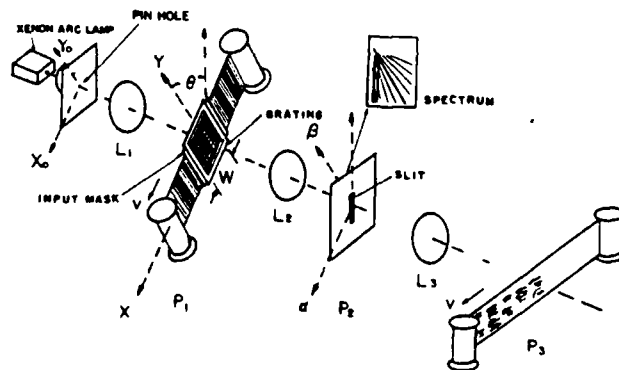


Fig. 2. White-light optical sound spectrograph. L , achromatic transform lens.

apparent that, if a slanted narrow slit is properly utilized at the Fourier plane, as illustrated in the figure, a frequency color-coded spectrogram can be recorded at the output plane, with a moving color film. The color-coded spectrographic signal can also be picked up by a color TV camera for displaying, storage, transmission, and further processing by electronic or digital system. We further note that, by simply varying the width of the input optical window, one would expect to obtain the so-called wideband and narrowband spectrograms. In other words, if a broader optical window is utilized for the spectrogram generation, a high spectral resolution, corresponding to a narrowband spectrogram, can be obtained.

However, by increasing the spectral resolution of the spectrogram, we would expect to lose the spatial (i.e., time) resolution. Conversely, if the optical window is narrower, which corresponds to a wideband analysis, a loss of spectral resolution is expected. However, loss of the spectral resolution improves the time resolution of the spectrogram. This time-bandwidth relationship is in fact, the consequence of the Heisenberg's uncertainty relation in quantum mechanics.⁹

For simplicity in analysis, we let the light source be a square white-light source. The source irradiance may be written as

$$\gamma(x_0, y_0; \lambda) = S(\lambda) \operatorname{rect}\left(\frac{x_0}{b}\right) \operatorname{rect}\left(\frac{y_0}{b}\right), \quad (3)$$

where $S(\lambda)$ is the spectral distribution of the light source, b denotes the size of the square source, and

$$\operatorname{rect}\left(\frac{x}{b}\right) = \begin{cases} 1, & |x| \leq b, \\ 0, & \text{otherwise.} \end{cases}$$

With reference to Wolf's partial coherence theory¹⁰ the mutual coherence function at the input plane P_1 of the spectrum analyzer of Fig. 2 would be

$$\begin{aligned} \Gamma(x_1, y_1; x_2, y_2; \lambda) &= \iint \gamma(x_0, y_0; \lambda) \\ &\cdot \exp\left\{-i \frac{2\pi}{\lambda f} [x_0(x_1 - x_2) \right. \\ &\quad \left. + y_0(y_1 - y_2)]\right\} dx_0 dy_0, \end{aligned} \quad (4)$$

where the integration is over the source irradiance. By carrying out the integration, the mutual coherence function at plane P_1 becomes

$$\begin{aligned} \Gamma(x_1, y_1; x_2, y_2; \lambda) &= KS(\lambda) \operatorname{sinc}\left[\frac{\pi b(x_1 - x_2)}{\lambda f}\right] \\ &\cdot \operatorname{sinc}\left[\frac{\pi b(y_1 - y_2)}{\lambda f}\right], \end{aligned} \quad (5)$$

where

$$\operatorname{sinc}(\pi\chi) \triangleq \frac{\sin(\pi\chi)}{\pi\chi},$$

and K is an appropriate constant.

Now, if the time-spatial signal format is inserted at the input plane P_1 of the processor, the mutual coherence function behind the input plane would be

$$\begin{aligned} \Gamma'(x_1, y_1; x_2, y_2; \lambda) &= \Gamma(x_1, y_1; x_2, y_2; \lambda) \exp[iq_0(y_1 - y_2)] \\ &\cdot t(x_1)t^*(x_2) \operatorname{rect}\left(\frac{x_1}{W}\right) \operatorname{rect}\left(\frac{x_2}{W}\right), \end{aligned} \quad (6)$$

where the exponential factor represents the phase transform of the 1-D phase grating, q_0 is the angular spatial frequency of the grating, $t(x)$ is the amplitude transmittance function of the recorded format, and W is the width of the input optical window as shown in the figure. Thus it is apparent that the mutual coherence function arriving at the Fourier plane P_2 would be

$$\begin{aligned} \Gamma(p_1, q_1; p_2, q_2; \lambda) &= \iiint \Gamma'(x_1, y_1; x_2, y_2; \lambda) \\ &\cdot \exp[-i(x_1 p_1 + y_1 q_1 - x_2 p_2 - y_2 q_2)] \\ &\cdot dx_1 dy_1 dx_2 dy_2, \end{aligned} \quad (7)$$

where the proportional constant is ignored for convenience, and (p, q) is the angular spatial frequency coordinate system which can be written as $p \triangleq 2\pi\alpha/\lambda$, $q \triangleq 2\pi\beta/\lambda$, and (α, β) is the spatial coordinate system of the Fourier plane P_2 .

By properly substituting Eq. (6) into Eq. (7) and integrating over the y_1 and y_2 variables, we have

$$\begin{aligned} \Gamma(p_1, q_1; p_2, q_2; \lambda) &= S(\lambda) \operatorname{rect}\left[\frac{\lambda f\left(\frac{q_1}{2} + \frac{q_2}{2} - q_0\right)}{2\pi b}\right] \cdot \delta(q_1 - q_2) \\ &\cdot \iint \operatorname{sinc}\left[\frac{\pi b(x_1 - x_2)}{\lambda f}\right] t(x_1)t^*(x_2) \\ &\cdot \operatorname{rect}\left(\frac{x_1}{W}\right) \operatorname{rect}\left(\frac{x_2}{W}\right) \\ &\cdot \exp[-i(x_1 p_1 - x_2 p_2)] dx_1 dx_2 \end{aligned} \quad (8)$$

For simplicity of illustration, we assume that the input format is a single sinusoidal signal, i.e.,

$$t(x) = 1 + \cos(p_0 x) \quad \text{for all } y, \quad (9)$$

where p_0 is the spatial frequency of the sinusoid. Since the cosine function of Eq. (9) can be written into two exponential functions, we focus our attention merely to one of the diffraction order, that is,

$$t(x_1)t^*(x_2) = \exp[ip_0(x_1 - x_2)] \quad (10)$$

By substituting Eq. (10) into Eq. (8), we obtain

$$\begin{aligned} \Gamma(p_1, q_1; p_2, q_2; \lambda) &= S(\lambda) \operatorname{rect}\left[\frac{\lambda f\left(\frac{q_1}{2} + \frac{q_2}{2} - q_0\right)}{2\pi b}\right] \cdot \delta(q_1 - q_2) \\ &\cdot \iint \operatorname{sinc}\left[\frac{\pi b(x_1 - x_2)}{\lambda f}\right] \exp[ip_0(x_1 - x_2)] \\ &\cdot \operatorname{rect}\left(\frac{x_1}{W}\right) \operatorname{rect}\left(\frac{x_2}{W}\right) \exp[-i(x_1 p_1 - x_2 p_2)] dx_1 dx_2. \end{aligned} \quad (11)$$

Since the interest is centered at the output irradiance, by letting $p_1 = p_2 = p$ and $q_1 = q_2 = q$, the irradiance at the Fourier plane would be

$$I(p, q; \lambda) = S(\lambda) \operatorname{rect}\left[\frac{\lambda f(q - q_0)}{2\pi b}\right] I(p), \quad (12)$$

where

$$\begin{aligned} I(p) &\triangleq \iint \operatorname{sinc}\left[\frac{\pi b(x_1 - x_2)}{\lambda f}\right] \exp[ip_0(x_1 - x_2)] \\ &\cdot \operatorname{rect}\left(\frac{x_1}{W}\right) \operatorname{rect}\left(\frac{x_2}{W}\right) \exp[-i(x_1 - x_2)p] dx_1 dx_2. \end{aligned} \quad (13)$$

To investigate the variation of the output irradiance due to the width of the input optical window, Fig. 3 shows a plot of the normalized intensity variation of Eq. (13) for two values of W . From this figure we see that a narrower spread of output irradiance corresponds to a broader optical window W at the input plane. Thus a narrowband spectrogram can be generated in this manner. On the contrary, if a narrower optical window is utilized, a broader spread of the output irradiance is

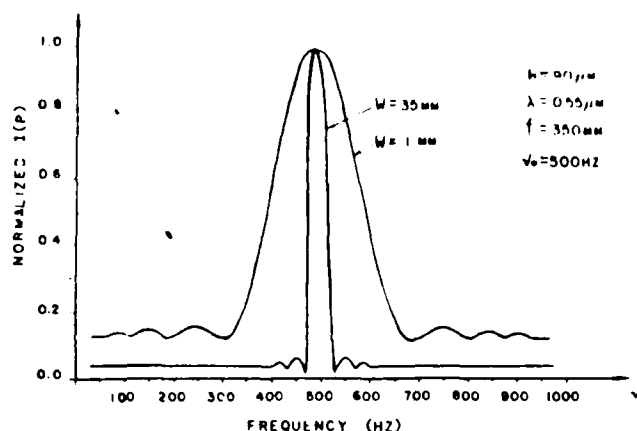


Fig. 3. Normalized output spectral distribution as a function of input frequency for two sizes of optical windows.

expected. Thus a wideband spectrogram may be generated with a narrow optical window.

To have a better understanding of Eq. (12), two extreme cases of the light source will be discussed in the following:

(a) If we assume that the broadband light source is vanishingly small (i.e., $b \rightarrow 0$), then

$$\lim_{b \rightarrow 0} \text{sinc} \left[\frac{\pi b(x_1 - x_2)}{\lambda f} \right] = 1,$$

and Eq. (12) takes the form

$$I(p, q; \lambda) = S(\lambda) \text{rect} \left[\frac{\lambda f(q - q_0)}{2\pi b} \right] \cdot W^2 \text{sinc}^2[\pi W(p - p_0)]. \quad (14)$$

This result describes a completely spatially coherent illumination.

(b) On the other hand, if the light source becomes infinitely large (i.e., $b \rightarrow \infty$), then

$$\lim_{b \rightarrow \infty} \text{sinc} \left[\frac{\pi b(x_1 - x_2)}{\lambda f} \right] = K \delta(x_1 - x_2),$$

where K is an appropriate constant, and Eq. (12) becomes

$$I(p, q; \lambda) = S(\lambda) \text{rect} \left[\frac{\lambda f(q - q_0)}{2\pi b} \right] W^2. \quad (15)$$

This result corresponds to a completely spatially incoherent illumination. Nevertheless, the proposed white-light spectrum analyzer, as can be seen, is operating in a partially coherent mode.

IV. Frequency Calibration and Resolution

We shall now discuss the frequency calibration of the proposed white-light optical speech spectrogram. The accuracy of the frequency measurement depends on the width of the input optical window as well as the width of the sampling slit at the Fourier plane. By adjusting these parameters, a properly calibrated speech spectrogram can be generated at the output plane.

Let us assume that the transform lenses are achromatic (i.e., $\partial f / \partial \lambda = 0$) and the angular spatial frequency of the input phase grating is q_0 . Thus we see that the

Fourier spectrum of the phase grating would be diffracted at

$$\beta = (\lambda / 2\pi) q_0, \quad (16)$$

where f is the focal length of the achromatic transform lens. Since Eq. (16) is linearly proportional to the wavelength of the light source, a rainbow color of smeared spectra can be observed along the β axis in the Fourier plane P_2 . For simplicity, we assume that input format is a single sinusoid of spatial frequency p_0 ; then the Fourier spectra points are located at

$$\alpha = \pm \frac{\lambda f}{2\pi} p_0. \quad (17)$$

For convenience, we use the positive value of Eq. (17) in our discussion. By taking the ratio of Eqs. (16) and (17), we have

$$\alpha = \frac{p_0}{q_0} \beta, \quad (18)$$

where we assume that $p_0 \ll q_0$, and q_0 is the spatial frequency of the phase grating. Thus we see that the frequency locus of the input signal can be properly traced out in the Fourier plane. In view of Eqs. (16) and (17), and the fact that $q_0 \gg p_0$, we further see that the spectrum of the input signal would disperse into a rainbow color at a slanted angle in the Fourier plane. It is, therefore, apparent that, if a narrow masking slit is properly utilized in the Fourier plane, a frequency color-coded spectrogram can be obtained at the output plane.

Now let us suppose that the masking slit can be described as

$$\beta = \frac{\lambda_0 f}{2\pi} q_0 + \alpha \tan \gamma, \quad (19)$$

where λ_0 denotes the upper or lower limit of the source wavelength depending on the slit orientation, and $\tan \gamma$ is the slope of the slit. By substituting Eqs. (16) and (17) into Eq. (19), we have

$$p_0 = \frac{q_0(\lambda - \lambda_0)}{\lambda \tan \gamma},$$

which can be written as

$$\nu = \frac{p_0 v}{2\pi} = \frac{q_0(\lambda - \lambda_0)v}{2\pi \lambda \tan \gamma}, \quad (20)$$

where ν is the time frequency of the input signal. Thus we see that the temporal frequency of the input signal and the spectral wavelength of the light source form a nonlinear function, as plotted in Fig. 4(a). Figure 4(b) shows the experimental result to confirm this relationship. Nevertheless this nonlinearity of frequency-spectral wavelength relationship can be linearized by using an appropriate curve slit instead of a linear one in the Fourier plane.

We shall now discuss the frequency resolution of the proposed system. We note that the frequency resolution is primarily limited by the width of the input optical window, the source size, and the width of the sampling slit in the Fourier plane. To investigate these effects, we assume that the size of the white-light source

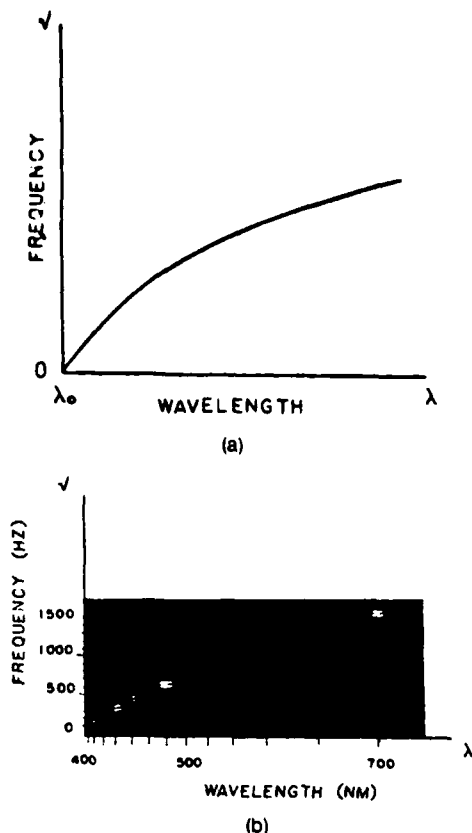


Fig. 4. Variation of input frequency vs spectral wavelength of the light source: (a) calculated result; (b) experimental result.

is b . Then the size of a point spread image would be

$$b' = b/f', \quad (21)$$

where f' and f are the focal lengths of collimating and achromatic Fourier transform lenses, respectively. Thus the width of the point spread image at the spatial frequency plane would be

$$\Delta\nu_1 = \frac{b'}{\lambda f'} = \frac{bv}{\lambda f'}. \quad (22)$$

Since the width of input optical window affects the spectral resolution of the processor, the width of the spectral lines in hertz for a point source is

$$\Delta\nu_2 = v/W, \quad (23)$$

where v is the speed of the film motion, and W is the width of the input optical window.

For simplicity, we shall treat these two factors (i.e., source size and width of optical window) independently. It is apparent that the spread of the smeared spectral line (i.e., frequency resolution) of the system can be approximated by the following equation:

$$\Delta\nu = [(\Delta\nu_1)^2 + (\Delta\nu_2)^2]^{1/2} = v \left[\left(\frac{b}{\lambda f'} \right)^2 + \left(\frac{1}{W} \right)^2 \right]^{1/2}. \quad (24)$$

As an example, if we let $v = 195$ mm/sec, $b = 90$ μ m, $\lambda = 0.55$ μ m, $W = 35$ mm, and $f' = 762$ mm, the frequency spread of the proposed optical spectrum analyzer is $\Delta\nu = 42$ Hz, which corresponds to a narrowband analysis

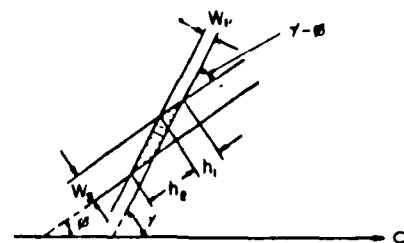


Fig. 5. Determination of the output spectral resolution.

(e.g., narrowband speech spectrogram). However, we see that the overall output resolution of the spectral spread is determined by the width and orientation of the sampling slit at the Fourier plane, as illustrated in Fig. 5. Thus the effective output frequency resolution can be shown as

$$\Delta\nu_e = \epsilon(h_1 + h_2) = \left[\frac{W_r}{\sin(\gamma - \phi)} + \frac{W_s}{\tan(\gamma - \phi)} \right], \quad (25)$$

where W_r and W_s are the width of the smeared frequency spectral line and the width of the sampling slit, ϵ is an appropriate conversion factor, and γ and ϕ are defined in the figure.

From this equation we see that the effective output frequency resolution is proportional to the diagonal region of the spectral line that intersects the sampling slit, as shown in the shaded area. Therefore, the overall output frequency resolution is somewhat lower than the width of the smeared spectral line, i.e.,

$$\Delta\nu_e \geq \Delta\nu. \quad (26)$$

This is the price of the color encoding. Nevertheless the price we paid is considered small compared with the advantages we gained from the white-light processing.

V. Experimental Demonstrations

In our experiments, a 75-W xenon arc lamp with a 90- μ m pinhole was used as a white-light source. A phase grating of 80 lines/mm was used as a dispersive element at the input plane. A narrow slit of ~ 70 μ m is inserted in the Fourier plane for color encoding. The focal length of the achromatic transform lens was ~ 350 mm.

In the experimental demonstration, we show two sets of color-coded speech spectrograms obtained with this technique, as depicted in Figs. 6 and 7. The frequency contents of these spectrograms are encoded in rainbow color from red to blue for upper to lower frequencies. These spectrograms were produced by a sequence of English words, testing, one, two, three, four, spoken by a male and a female voice, respectively. Figure 6 shows a set of narrowband speech spectrograms representing a 45-Hz bandwidth resolution. Figure 7 illustrates a set of wideband speech spectrograms with a 300-Hz bandwidth analysis. From these sets of spectrograms, we see that the basic structure of the spectrographic contents is preserved. The characterization of the formant variation can readily be identified. Since Fig. 6(a) is produced by a low-pitched voice (i.e., male), the

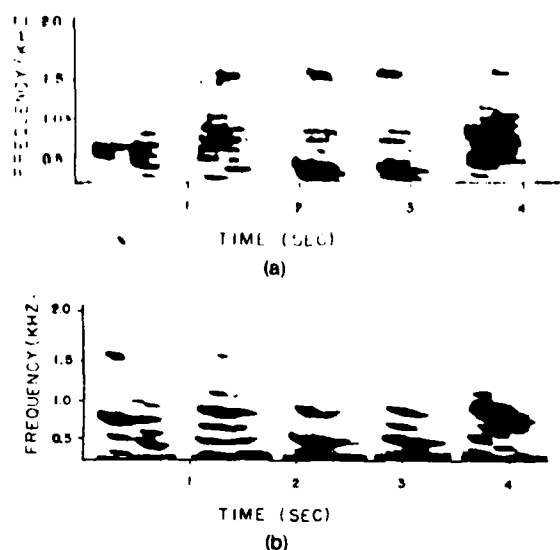


Fig. 6. Black-and-white photographs of narrowband color-coded speech spectrograms (~ 45 -Hz bandwidth): (a) obtained with a male voice; (b) obtained with a female voice.

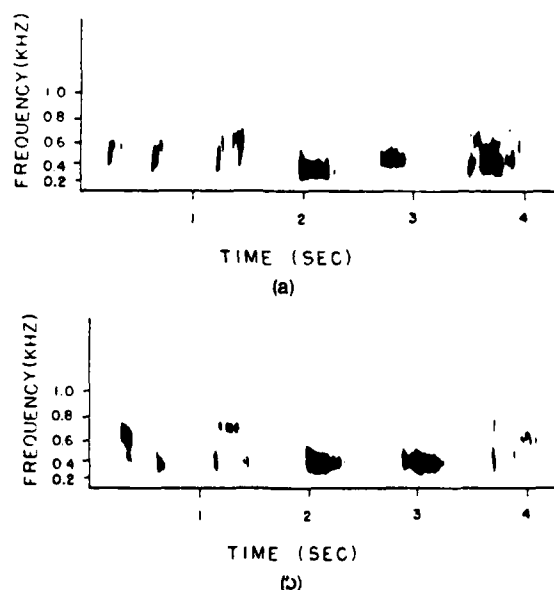


Fig. 7. Black-and-white pictures of wideband color-coded speech spectrograms (~ 300 -Hz bandwidth): (a) generated by a male voice; (b) generated by a female voice.

spectrogram shows more abundant harmonics as compared with the high-pitched voice in Fig. 6(b).

It is worthwhile to mention that although the narrowband spectrogram is capable of resolving the spectral contents of a speech, it loses the time striation, as can be seen in Fig. 6. On the other hand, the wideband

spectrograms of Fig. 7 are capable of resolving the time resolution, but it fails to resolve the spectral lines. We note that the trading of time and frequency resolutions between the wide and narrow spectrograms is essentially the well-known $\Delta\nu\Delta t \geq 1$ concept in the communication theory (i.e., $\Delta\nu\Delta t \geq 1$), which is related to the famous Heisenberg's uncertainty principle⁹ in quantum mechanics.

VI. Conclusion

In this paper, we have presented a method of generating a continuous frequency color-coded speech spectrogram with a white-light processing technique. The proposed system not only offers a low-cost alternative but also eliminates the coherent artifact noise. Moreover, the multicolor display of the spectrogram is adapted to the natural sensitivity of human eyes and thereby provides improved visual discrimination. Nevertheless, we want to stress that due to the very limited resolution of the CRT scanner used in our experiments, the results that we obtained only extended to 1.6 kHz. This limitation is more pronounced for a wideband spectrographic analysis, which is primarily due to low-light performance of narrower optical window used at the object plane. However, to our experience, if a higher-resolution CRT scanner is utilized, the frequency range can easily push up to 4 kHz. This frequency range is commonly used for most telephonic systems.

References

1. W. Koenig, H. K. Dunn, and L. Y. Lacy, "The Sound Spectrograph," *J. Acoust. Soc. Am.* 18, 19 (1946).
2. L. J. Cutrona, E. Leith, C. Palermo, and J. Porcello, "Optical Data Processing and Filtering Systems," *IRE Trans. Inf. Theory* IT-6, 386 (1960).
3. C. E. Thomas, "Optical Spectrum Analysis of Large Space Bandwidth Signals," *Appl. Opt.* 5, 1782 (1966).
4. F. T. S. Yu, "Synthesis of an Optical-Sound Spectrograph," *J. Acoust. Soc. Am.* 51, 433 (1972).
5. F. T. S. Yu, "Generating Speech Spectrograms Optically," *IEEE Spectrum*, 12, 51 (Feb. 1975).
6. E. B. Felstead, "Optical Fourier Transformation of Area-Modulated Spatial Functions," *Appl. Opt.* 10, 2468 (1971).
7. K. R. Hessel, "Some Theoretical Limitations of the Optical Power Spectrum Analyzer," *Appl. Opt.* 13, 1023 (1974).
8. F. T. S. Yu, "Information Content of a Sound Spectrogram," *J. Audio Eng. Soc.* 15, 407 (1967).
9. F. T. S. Yu, *Optics and Information Theory* (Wiley-Interscience, New York, 1976).
10. M. Born and E. Wolf, *Principles of Optics* (Pergamon, New York, 1980).

We acknowledge the support of U.S. Air Force Office of Scientific Research grant AFOSR-83-0140.

SECTION VIII

Progress on Archival Color Film Storage

ELECTRICAL ENGINEERING DEPARTMENT, THE PENNSYLVANIA STATE UNIVERSITY

University Park, Pennsylvania 16802 (USA)

PROGRESS REPORT ON ARCHIVAL STORAGE OF COLOR FILMS UTILIZING A WHITE-LIGHT PROCESSING TECHNIQUE

F. T. S. YU, X. X. CHEN and S. L. ZHUANG

MOTS CLÉS :

Traitement d'image
Codage couleur

KEY WORDS :

Image processing
Color encoding

SUMMARY : In this paper, we report a spatially encoding technique such that the moiré fringe pattern inherently existing with the retrieved image can be avoided. To improve the diffraction efficiency of the film, we have introduced a bleaching process so that the step of obtaining a positive encoded transparency can be eliminated. Instead of restricting the encoding processing in the linear region of the T - E curve, we would allow the encoding in the linear region of the D - E curve, so that a broader range of encoding exposure can be utilized. Experimental results indicate that excellent color fidelity, high signal to noise ratio, and good resolution of the reproduced color images can be obtained.

Amélioration d'une technique de traitement en lumière blanche pour l'archivage de films en couleurs

RÉSUMÉ : Dans cet article nous décrivons une technique de codage spatial qui évite les effets de moiré dans l'image restituée. Pour améliorer l'efficacité du réseau de diffraction formé par le film, nous avons introduit une technique de blanchiment qui élimine le tirage d'un positif. Au lieu de restreindre le codage dans la partie linéaire de la courbe transmission-éclairage, il est possible de coder sur la partie linéaire de la courbe efficacité de diffraction-éclairage, ce qui élargit la gamme d'expositions. Les résultats expérimentaux montrent une excellente fidélité des couleurs, un grand rapport signal sur bruit et une bonne résolution dans la restitution des images en couleurs.

INTRODUCTION

Archival storage of color films has long been an unresolved problem for the film industry. The major reason is that the organic dyes used in color films are usually unstable under prolonged storage, often causing gradual color fading. Although there are several available techniques for preserving the color images, all of them possess certain definite drawbacks. One of the most commonly used techniques involves repetitive application of primary color filters, so that the color images can be preserved, in three separate rolls of black-and-white film. To retrieve the color image, a system with three primary color projectors are used. These films should be projected in perfect unison so that the primary color images will be precisely recorded on a fresh roll of color film. However, this technique has two major drawbacks : first, the storage volume for each film is tripled. Second, the reproduction system is rather elaborate and expensive.

The use of monochrome transparencies to retrieve

color images was first reported by Ives [1] in 1906. He introduced a slide viewer that produced color images by a diffraction phenomenon. Grating either of different spatial frequencies or of azimuthal orientations were used. More recently, Mueller [2] described a similar technique, employing a tricolor grid screen for image encoding. In decoding, he used three quasi-monochromatic sources for color image retrieval. Since then, similar work on color image retrieval has been reported by Macovski [3], Grousson and Kinany [4], and Yu [5]. However, those techniques suffer a major drawback : namely, the moiré fringes in the retrieval color image will not be avoided.

We will, in this paper, report a spatially encoding and decoding process such that the moiré fringe pattern can be avoided by spatial filtering. To improve the diffraction efficiency, we have introduced a bleaching processing for the encoded film in which the step of generating a positive transparency can be eliminated. We have also experimentally demonstrated that the spatially encoding process should not be restricted to the linear region of the H - D curve.

Instead, it is recommended to encode in the linear region of the diffraction efficiency *versus* exposure curve (called *D-E* curve). Detail experimental procedure of this archival storage technique is presented. Preliminary results of retrieval color images are provided. Comparisons with original color transparency are also given.

SPATIAL ENCODING AND DECODING

We shall now describe a spatial encoding technique utilizing a white-light source. A color transparency is used as an object to be encoded, by sequentially exposing with primary color of lights, onto a black-and-white film, as illustrated in *figure 1*. The encoding is taken place by spatial sampling; the primary color images of the color transparency, with a specific sampling frequency and a prescribed direction onto a monochrome film. In order to avoid the moire fringe pattern in the retrieval color image, we propose to sample one of the primary color images in one independent spatial coordinate, and the remaining two primary color images in the other independent spatial coordinate, as shown in *figure 2*. Since any mixture of red with green or with blue colors produces a wide range of intermediate colors, we propose to encode the red color image in one independent spatial coordinate direction, and the blue and green color images in the other remaining independent coordinate direction. Thus a small amount of color spread (i.e., color crosstalk) from blue to green (but not from green to blue) may not be avoided. However this small amount of color spread will not cause significant adverse effect in the retrieved color image, for primarily two reasons: first, a slight mixture of blue into green will not produce significant color changes. Second, strictly speaking all the color transparencies are not natural colors, thus a small amount of color deviation would not be noticeable by human perception.

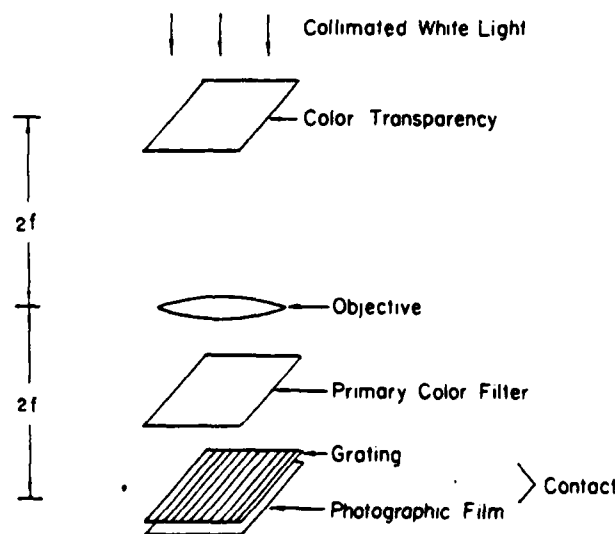


FIG. 1. — Sequential spatial color encodings.

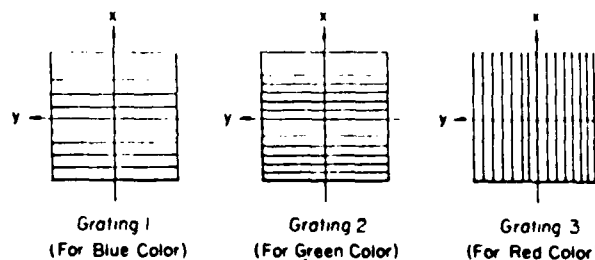


FIG. 2. — Positions of the three spatial samplings.

We shall now demonstrate that the moire fringes can be avoided with the proposed encoding-decoding technique. Let this intensity transmittance of the encoded films be [5]

$$T_e(x, y) = K \{ T_r(x, y) [1 + \text{sgn}(\cos p_r y)] + T_b(x, y) [1 + \text{sgn}(\cos p_b x)] + T_g(x, y) [1 + \text{sgn}(\cos p_g x)] \}^{-\gamma}, \quad (1)$$

where $T_e(x, y)$ is the encoded black-and-white negative transparency, K is an appropriate proportionality constant, T_r , T_b and T_g are the red, blue, and green color image exposures, p_r , p_b , and p_g are the respective carrier spatial frequencies, (x, y) is the spatial frequency coordinate system of the encoded film, γ is the film gamma [6], and

$$\text{sgn}(\cos x) \triangleq \begin{cases} 1, & \cos x \geq 0, \\ -1, & \cos x < 0. \end{cases} \quad (2)$$

Instead of obtained a positive image transparency, through a contact printing process of Eq. (2) as proposed in a previous paper [5], we shall bleach the encoded negative-image film to obtain a phase object transparency [7, 8]. Let us assume that the bleached transparency is encoded in the linear region of the diffraction efficiency *D* *versus* exposure *E* (e.g., as shown in *fig. 6*). The amplitude transmittance of the bleached transparency can be written

$$t(x, y) = \exp[i\phi(x, y)], \quad (3)$$

where $\phi(x, y)$ represents the phase delay distribution, which is proportional to the exposure of the encoded film [9], such as

$$\phi(x, y) = M \{ T_r(x, y) [1 + \text{sgn}(\cos p_r y)] + T_b(x, y) [1 + \text{sgn}(\cos p_b x)] + T_g(x, y) [1 + \text{sgn}(\cos p_g x)] \}, \quad (4)$$

where M is an appropriate proportionality constant. If we place this bleached encoded film at the input plane P_1 of a white-light optical processor, as illustrated in *figure 3*, then the complex light distribution due to $t(x, y)$, for every λ , at the spatial frequency plane P_2 can be determined by the following Fourier

transformation :

$$\begin{aligned} S(\alpha, \beta; \lambda) &= \iint t(x, y) \exp \left[-i \frac{2\pi}{\lambda f} (\alpha x + \beta y) \right] dx dy \\ &= \iint \exp[i\phi(x, y)] \exp \left[-i \frac{2\pi}{\lambda f} (\alpha x + \beta y) \right] dx dy. \end{aligned} \quad (5)$$

By expanding $t(x, y)$ into exponential series, Eq. (5) can be written

$$S(\alpha, \beta; \lambda) = \iint \left\{ 1 + i\phi(x, y) + \frac{1}{2} [i\phi(x, y)]^2 + \dots \right\} \exp \left[-i \frac{2\pi}{\lambda f} (\alpha x + \beta y) \right] dx dy. \quad (6)$$

By substituting Eq. (4) into Eq. (6) and retaining the first-order and the first-order convolution terms we have :

$$\begin{aligned} S'(\alpha, \beta; \lambda) &= \hat{T}_r \left(\alpha, \beta \pm \frac{\lambda f}{2\pi} p_r \right) + \hat{T}_b \left(\alpha \pm \frac{\lambda f}{2\pi} p_b, \beta \right) \\ &\quad + \hat{T}_g \left(\alpha \pm \frac{\lambda f}{2\pi} p_g, \beta \right) + \hat{T}_r \left(\alpha, \beta \pm \frac{\lambda f}{2\pi} p_r \right) * \hat{T}_b \left(\alpha \pm \frac{\lambda f}{2\pi} p_b, \beta \right) \\ &\quad + \hat{T}_r \left(\alpha, \beta \pm \frac{\lambda f}{2\pi} p_r \right) * \hat{T}_g \left(\alpha \pm \frac{\lambda f}{2\pi} p_g, \beta \right) + \hat{T}_b \left(\alpha \pm \frac{\lambda f}{2\pi} p_b, \beta \right) * \hat{T}_g \left(\alpha \pm \frac{\lambda f}{2\pi} p_g, \beta \right). \end{aligned} \quad (7)$$

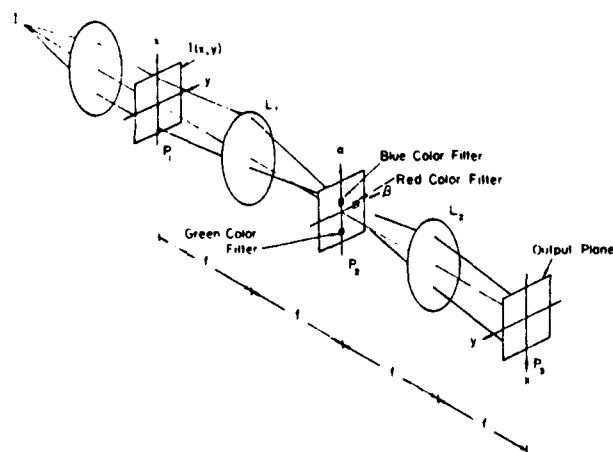


FIG. 3. — White light processor for spatial color decoding. 1, extended white light source; L_1 , transform lens; $T(x, y)$, bleached encoded transparency.

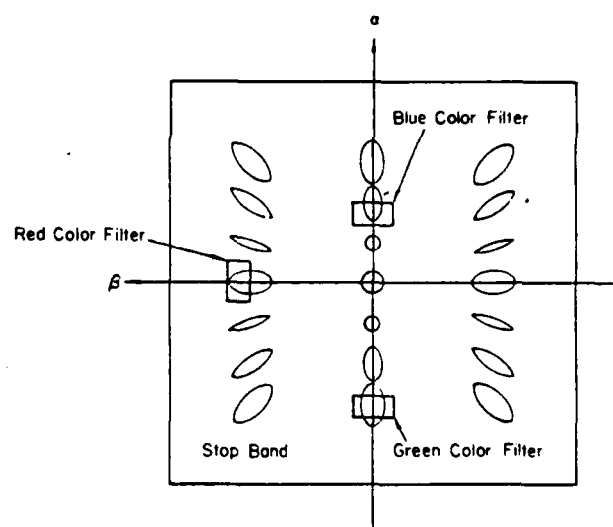


FIG. 4. — Color spatial filtering at the spatial frequency plane.

where \hat{T}_r , \hat{T}_b and \hat{T}_g are the Fourier transforms of T_r , T_b and T_g respectively. * denotes the convolution operation, and the proportional constants have been neglected for simplicity. We note that, the last cross product term of Eq. (7) would introduce a moiré fringe pattern, parallel to encoding gratings of blue and green, in the retrieved color image. Nevertheless, all of those cross product terms can be properly masked out at the Fourier plane. Thus by proper color filtering those first-order smeared Fourier spectra, as shown in figure 4, a moiré free true color image can be retrieved at the output image plane P_3 . The corresponding complex light field immediately behind

the Fourier plane would be

$$\begin{aligned} S(\alpha, \beta) &= \hat{T}_r \left(\alpha, \beta - \frac{\lambda_r f}{2\pi} p_r \right) \\ &\quad + \hat{T}_b \left(\alpha - \frac{\lambda_b f}{2\pi} p_b, \beta \right) + \hat{T}_g \left(\alpha + \frac{\lambda_g f}{2\pi} p_g, \beta \right) \end{aligned} \quad (8)$$

where λ_r , λ_b , and λ_g are the respective red, blue, and green color wavelengths. At the output image plane, the complex light distribution is

$$s(x, y) = T_r(x, y) \exp(i\gamma p_r) + T_b(x, y) \exp(i\gamma p_b) + T_g(x, y) \exp(-i\gamma p_g). \quad (9)$$

The output image irradiance is therefore

$$I(x, y) = I_r^2(x, y) + I_g^2(x, y) + I_b^2(x, y), \quad (10)$$

which is a superposition of three primary encoded color images. Thus we see that a moire free color image can indeed be obtained.

We shall now discuss the effect of moire fringe pattern in more detail. It is well known that a moire pattern is produced by the overlaying of two or more gratings [10, 11]. When two gratings of spacing a and b are superimposed with an obliquity angle of θ , the moire fringe spacing d can be written as :

$$d = \frac{hab}{\sqrt{a^2 + b^2 - 2ab \cos \theta}} \quad (11)$$

and this slope of the moire fringe is

$$\tan \phi = \frac{b \sin \theta}{a - b \cos \theta}, \quad (12)$$

where h is the index of moire pattern ($h = 0, \pm 1, \pm 2, \dots$) which represents the resultant moire fringes as an indexed family of curves (see ref. 11). If these two gratings are perpendicularly superimposed at an angle $\theta = 90^\circ$, then they form a cross grating pattern, without moire fringes [11].

On the other hand, if two gratings are parallel-superimposed on the top of the other (i.e., $\theta = 0^\circ$), then a beating frequency parallel to those gratings would occur. The corresponding fringe spacing is

$$d = \frac{hab}{|a - b|}, \quad (13)$$

and the relevant (i.e., moire) spatial frequency is

$$p_m = \frac{2\pi}{d} = |p_a - p_b|, \quad (14)$$

where $p_a = 2\pi/a$ and $p_b = 2\pi/b$ are the spatial frequencies of the two gratings.

We shall now investigate the moire fringe effects due the spatial encoding of figure 2. Since grating no. 3 is perpendicularly superimposed with grating

nos. 1 and 2, it will not generate any undesirable moire fringes except a cross grid between gratings 3 and 1, and 3 and 2. Whereas gratings 1 and 2 are parallel-superimposed, it produces a moire fringe pattern of spatial frequency $p_m = |p_b - p_a|$ in the same direction of gratings 1 and 2.

Since the last term of Eq. (7) represents the Fourier transform of this moire fringe pattern, the resolution of the retrieved encoded color image (blue or green) is limited by the size of the color spatial filters, as illustrated in figure 4. Therefore, the spatial frequency requirements of the gratings 1 and 2 can be determined by the following equation

$$p_g = \frac{1}{2}(p_g + 2p_b) = \frac{3}{2}p_b. \quad (15)$$

The resolution limit of retrieved color image is

$$p = |p_g - p_b| = \frac{1}{2}p_b, \quad (16)$$

and the spatial frequency of the moire fringe pattern is

$$p_m = |p_g - p_b| = \frac{1}{2}p_b. \quad (17)$$

Thus, by proper selection of desirable grating frequencies, which depends upon the resolution limit of the object transparency, the spatial frequency content of the moire pattern can be determined. With appropriate color filtering, the encoded Fourier spectra as illustrated in figure 4, a moire free color image can be obtained.

EXPERIMENTAL DEMONSTRATION

In our experiment, we utilized three Kodak primary color filters of No. 25, 47B and 58 for the encoding and decoding process. The characterizations of these filters, illuminated by standard A illuminant [12, 13], are specified by the C.I.E. diagram, as shown in figure 5. The corresponding trichromatic coefficients of these filters are tabulated in the following :

No. 25 - R^* : $\lambda = 6150 \text{ \AA}$	$x_R = 0.680$	$y_R = 0.320$	$z_R = 0$
No. 58 - G^* : $\lambda = 5500 \text{ \AA}$	$x_g = 0.302$	$y_g = 0.692$	$z_g = 0.006$
No. 47B - B^* : $\lambda = 4300 \text{ \AA}$	$x_b = 0.169$	$y_b = 0.007$	$z_b = 0.824$
and W_A^* :	$x_w = 0.448$	$y_w = 0.408$	$z_w = 0.144$

(18)

where R^* , G^* , B^* and W_A^* denote the red, green, blue and white colors, respectively, $x + y + z = 1$, and x , y , and z are the trichromatic coefficients obtained from the chromaticity coordinates of the C.I.E. chromaticity diagram [12, 13]. Grating frequency of 40 lines/mm is used for red and green color image encodings, and grating frequency of 26.7 lines/mm is used for blue color image encoding. A xenon arc lamp is used for the white-light processing, and the color

decoding filters are the same type of color filters used for the encoding. The trichromatic coefficients are expected to be the same as those in Eq. (18), except for the white color, that is

$$W_c^* : x_w = 0.310, \quad y_w = 0.316, \quad z_w = 0.374. \quad (19)$$

We shall now illustrate that any choice of color can be reproduced by a simple transformation from C.I.E.

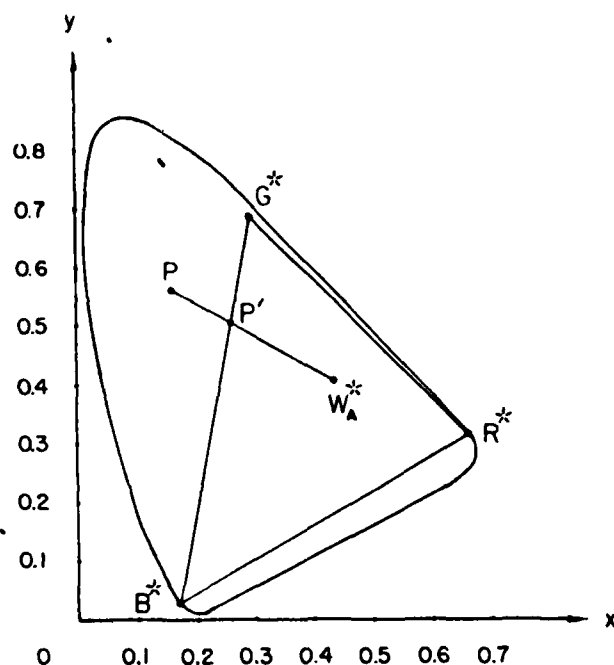


FIG. 5. — Chromaticity coordinates in C.I.E.

to $R^* G^* B^*$ as described in the following equation [14, 15].

$$\begin{aligned} R &= K_1 X + K_2 Y + K_3 Z, \\ G &= K_4 X + K_5 Y + K_6 Z, \end{aligned} \quad (20)$$

and $B = K_7 X + K_8 Y + K_9 Z,$

where R , G , and B are the red, green, and blue color tristimulus values, and X , Y , and Z are the C.I.E. tristimulus values, and the K 's are arbitrary constants. We note that these tristimulus values can be expressed as [14, 15]:

$$\begin{aligned} R &= y_w \begin{vmatrix} X & x_G & x_B \\ Y & y_G & y_B \\ Z & z_G & z_B \end{vmatrix} \begin{vmatrix} x_W & x_G & x_B \\ y_W & y_G & y_B \\ z_W & z_G & z_B \end{vmatrix}^{-1}, \\ G &= y_w \begin{vmatrix} x_R & X & x_B \\ y_R & Y & y_B \\ z_R & Z & z_B \end{vmatrix} \begin{vmatrix} x_R & x_W & x_B \\ y_R & y_W & y_B \\ z_R & z_W & z_B \end{vmatrix}^{-1}, \\ B &= y_w \begin{vmatrix} x_R & x_G & X \\ y_R & y_G & Y \\ z_R & z_G & Z \end{vmatrix} \begin{vmatrix} x_R & x_G & x_W \\ y_R & y_G & y_W \\ z_R & z_G & z_W \end{vmatrix}^{-1}, \end{aligned} \quad (21)$$

and

where the x s and y s are the trichromatic coefficients. By substituting the trichromatic coefficients of Eq. (18) into Eq. (21), we have

$$\begin{aligned} R &= 1.688 X - 0.734 Y - 0.340 Z, \\ G &= -0.915 X + 1.944 Y + 0.171 Z, \end{aligned} \quad (22)$$

and $B = 0.014 X - 0.031 Y + 2.810 Z.$

The chromaticity coordinates can be determined in the following definitions:

$$\begin{aligned} r &\triangleq \frac{R}{R+G+B} = \frac{1.688 X - 0.734 Y - 0.340 Z}{0.787 X + 1.179 Y + 2.641 Z}, \\ g &\triangleq \frac{G}{R+G+B} = \frac{-0.915 X + 1.944 Y + 0.171 Z}{0.787 X + 1.179 Y + 2.641 Z}, \end{aligned} \quad (23)$$

and

$$b \triangleq \frac{B}{R+G+B} = \frac{0.014 X - 0.031 Y + 2.810 Z}{0.787 X + 1.179 Y + 2.641 Z},$$

where r , g , and b are the chromaticity coordinates. Thus, any choice of color can be one-to-one homologically reproduced with this color transformation.

Although the color retrieval is evaluated within the triangle defined by $R^* G^* B^*$ of figure 5, any color point outside the triangle can be replaced by the nearness neighboring point on the boundary of the triangle, for example, p can be replaced by p' . Since the hue is generally keeping it up, it will not introduce significant adverse effect by human perception. In practice, we need only to control the exposure ratio of the encodings such that white color object can be retrieved by a white-light processor. With reference to these available exposure ratios, a broad dynamic range of encodings onto a typical photographic plate can then be achieved, as shown in figure 6.

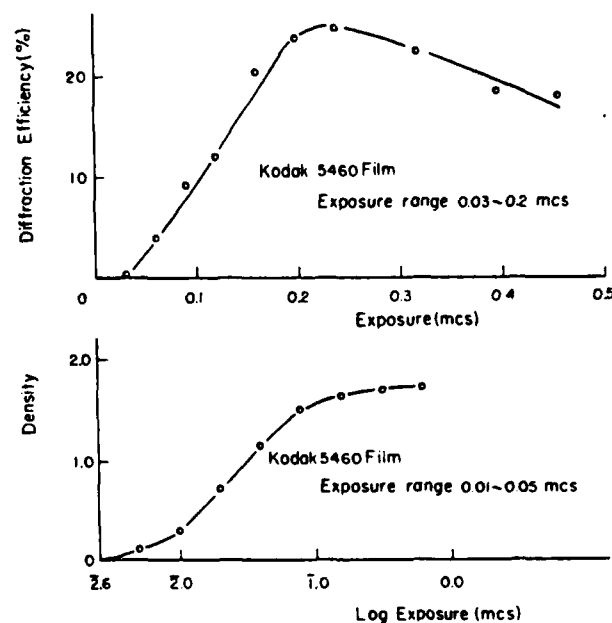


FIG. 6. — A broad exposure range of encodings.

In our experiment, the encoding transparencies are made by Kodak technical pan film 2415 and Kodak Microfilm 5460. The advantage of using Kodak film 2415 is that it is a low contrast film with a relatively flat spectral response, as shown in figure 7. The disadvantage is that this film is coated with a thin layer of dyed-gel backing, for which it introduces additional noise through the bleaching process. Although the microfilm used is a clear base film, however, it is a high gamma film and the spectral response decreases somewhat in the red color region, as shown in figure 7. In order to compensate this low spectral response, one would encode the red wavelength with a higher exposure. Needless to say that, the resolution and contrast of the retrieval color image are also affected by this developing process of the film.

It should emphasize that, to avoid the shoulder region of the $D-E$ curve, the film should be preexposed. Otherwise, it would introduce low exposure nonlinear effect which causes color unbalance in the retrieval image. The plots of diffraction efficiency versus exposure for Kodak 2415 and 5460 films with 40 lines/mm sampling frequency, are plotted in figure 8. From the figure, we see that the bleached encoded films offer a higher diffraction efficiency, the optimum value occurs at exposures 8.50×10^{-3} mcs and 1.95×10^{-1} mcs, respectively for Kodak films 2415 and 5460. With these optimum exposures, it is possible to optimize the encoding process in the following: first, by preexposing the film beyond the toe region. Second, by subdividing the remaining exposure, taken the account of the film spectral response, into three parts for the red, green, and blue color images.

For experimental demonstrations, we would like to provide two results obtained by Kodak 2415 and Kodak 5460 encoding films, as shown respectively in figures 9a and 9b. From these figures we see that the moiré free color images can indeed be obtained. We also see that the retrieved color image, obtained by this Kodak Microfilm 5460, provides a higher image quality (i.e., higher resolution and lower noise level). The primary reason is that, commercially available, Kodak 2415 is coated with a thin layer of dyed-gel backing. Accordingly, this thin layer of dyed-gel backing causes additional noise level through bleaching process. For comparison, we also provide

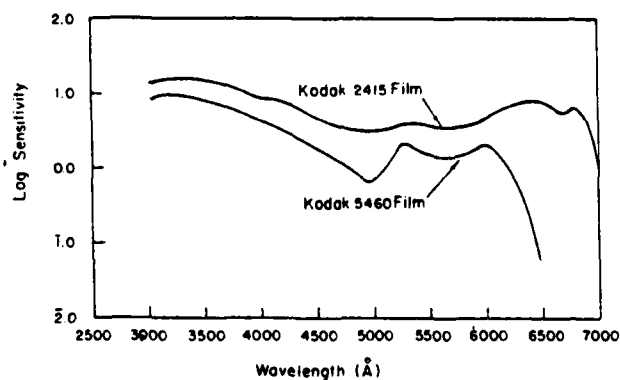


FIG. 7. — Spectral responses of Kodak films 2415 and 5460.

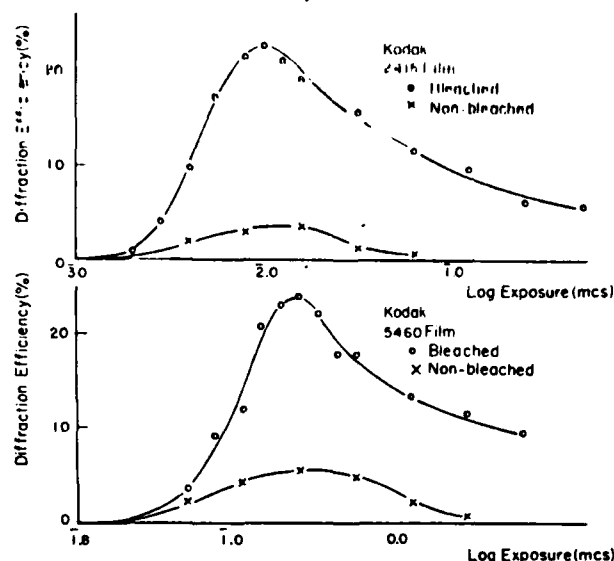


FIG. 8. — The plots of diffraction efficiency versus exposure for Kodak film 2415 and 5460 for a 40 lines/mm sampling.

the original color transparency as shown in figure 10. By comparing the results of figure 9 with figure 10, we see that the retrieval color images are spectacularly faithful, with virtually no color cross-talk. Although the resolution and contrast are still far below the acceptable stage for applications, however these drawbacks may be overcome by utilizing a more suitable film, for which a research program is currently under investigation. We are confident that better results would be obtained from our future research in this program.

CONCLUSION

In conclusion, we would like to point out that, a technique of spatial encoding for archival storage of color films utilizing a white-light processing is presented. The encoding is taken place with red color image on one independent coordinate, and blue and green color images on another independent coordinate, so that the moiré free color image can be retrieved at the output plane. We have also introduced a bleaching process to convert a negative encoded image into a phase object encoded transparency, in which the step of generating a positive encoded transparency can be avoided. Experimental results show that spectacularly faithful color images can be obtained with the technique. Although the resolution and contrast are still below the general acceptable stage for practical application, however by using a more suitable encoding film these drawbacks may be eliminated.

We acknowledge the support of the U.S. Air Force Office of Scientific Research grant AFOSR-81-0148.



a)



b)

FIG. 9. — Color pictures reproduced by this technique.

- (a) obtained by Kodak 2415;
- (b) obtained by Kodak 5460.



FIG. 10. — Color picture of the original color image.

REFERENCES

- [1] IVES (H. E.). — *Br. J. Photog.*, 609 (1906).
- [2] MUELLER (P. Y.). — *Appl. Opt.*, 8, 2051 (1969).
- [3] MACOVSKI (A.). — *Appl. Opt.*, 11, 416 (1972).
- [4] GROUSSON (R.), KINANY (R. J.). — *J. Opt.*, 9, 333 (1978).
- [5] YU (F. T. S.). — *Appl. Opt.*, 19, 2457 (1980).
- [6] YU (F. T. S.). — *Optical Information Processing*, Wiley-Interscience Publishing Co., New York, 1982.
- [7] UPATNIEKS (J.), LEONARD (C.). — *Appl. Opt.*, 8, 85 (1969).
- [8] CHANG (B. J.), WINICK (K.). — *SPIE*, 215, 172 (1980).
- [9] SMITH (H. M.). — « Basic Holographic Principles », Ed. : H. M. Smith, *Holographic Recording Materials*, Springer-Verlag, New York, 1977.
- [10] GUILD (J.). — *The Interference System of Crossed Diffraction Gratings*, Oxford University Press, London, 1956.
- [11] OSTER (G.). — *Symposium in Quasi-Optics*, Polytechnic Press, Brooklyn, NY, 1964.
- [12] *Kodak Filters for Scientific and Technical Use*, Eastman Kodak Company, 1st ed., NY, 1970, p. 18.
- [13] COMPTON (K. T.). — *Handbook of Colorimetry*, MIT Press, Cambridge, 1936.
- [14] *The Science of Color*, published by Optical Society of America, 1963.
- [15] FINK (D. G.) — Ed., *Color Television Standards*, McGraw-Hill Book Company, NY, 1955.

(Manuscript received in May 15, 1984)

SECTION IX

Recent Advances on White-Light Image Processing

Recent Advances in White-Light Image Processing

FRANCIS T. S. YU

*Department of Electrical Engineering
The Pennsylvania State University
University Park, Pennsylvania*

I. Introduction	1
II. White-Light Optical Image Processing	3
III. Coherence Requirement	7
A. Propagation of Mutual Coherence Function	8
B. General Formulation	12
C. Coherence Requirement for Image Deblurring	15
IV. Coherence Measurement	24
A. Measurement Technique	24
B. Coherence Measurement	27
C. Summary	36
V. Source Encoding, Image Sampling and Filtering	36
A. Source Encoding	37
B. Image Sampling and Filtering	39
C. An Illustrative Application	40
VI. Advances in Image Processing	43
A. Color Image Deblurring	43
B. Color Image Subtraction	46
C. Color Image Retrieval	51
D. Pseudocolor Encoding	55
E. Real-Time Pseudocolor Encoding	63
VII. Concluding Remarks	68
Reference	69

I. INTRODUCTION

Signal processing originated with a group of electrical engineers whose interest was mainly centered on electrical communication. Nonetheless, from the very beginning of the development of signal processing, the interest in its application to image processing has never been totally disregarded. In recent

demonstrated that the white-light image processor is very economical and easy to operate, in contrast with coherent counterparts. Therefore we would expect that the white-light image processor would offer a broader range of application to many scientific imageries.

In this chapter, we have also described some of the recent advances in white-light image processing. We have demonstrated that color image deblurring, color image subtraction, color image retrieval, and pseudocolor encoding can be easily carried out by the proposed white-light processing technique. We have also shown that these white-light image processing operations can be evaluated from the stand point of conventional linear systems.

In spite of the flexibility of digital image processing, optical methods offer the advantage of capacity, color, simplicity, and cost. Instead of confronting each other, we can expect a gradual merging of the optical and digital techniques. The continued development of optical-digital interfaces and various electro-optics devices will lead to a fruitful result: hybrid optical-digital image processing techniques, utilizing the strengths of both processing operations. Furthermore, I believe that white-light image processing is at the threshold of widespread application. I hope that this chapter will serve a basic foundation, already established in part, to help guide interested readers toward various imaginative image processing applications. In view of the great number of contributors, I apologize for possible omissions of appropriate references.

ACKNOWLEDGMENTS

The support of the U.S. Air Force Office of Scientific Research in the area of white-light optical processing is gratefully acknowledged.

REFERENCES

1. D. Gabor, Laser speckle and its elimination. *IBM J. Res. Dev.* **14**, 509 (1970).
2. F. T. S. Yu, "Optical Information Processing." Wiley (Interscience), New York, 1983.
3. G. L. Rogers, Non-coherent optical processing. *Opt. Laser Technol.* **7**, 153 (1975).
4. K. Bromley, An optical incoherent correlation. *Opt. Acta* **21**, 35 (1974).
5. M. A. Monahan, K. Bromley, and R. P. Bocker, Incoherent optical correlations. *Proc. IEEE* **65**, 121 (1977).
6. G. L. Rogers, "Noncoherent Optical Processing." Wiley, New York, 1977.

X. LIST OF PUBLICATIONS RESULTING FROM AFOSR SUPPORT

1. S. T. Wu and F. T. S. Yu, "Source Encoding for Image Subtraction," Optics Letters, Vol. 6, pp. 452-454, September, 1981.
2. F. T. S. Yu and J. L. Horner, "Optical Processing of Photographic Images," Optical Engineering, Vol. 20, pp. 666-676, September-October 1981.
3. F. T. S. Yu, "Partially Coherent Optical Processing of Images," SPIE Proceedings on "Processing Images and Data from Optical Sensors," Vol. 292, pp. 2-8, 1982.
4. F. T. S. Yu and J. L. Horner, "Review of Optical Processing of Images," SPIE Proceedings on Processing Images and Data from Optical Sensors," Vol. 292, pp. 9-24, 1982.
5. F. T. S. Yu, S. L. Zhuang and T. H. Chao, "Color Photographic-Image Deblurring by White-Light Processing Technique," Journal of Optics, Vol. 13, pp. 57-61, March-April, 1982.
6. S. T. Wu and F. T. S. Yu, "Image Subtraction with Encoded Extended Incoherent Source," Applied Optics, Vol. 20, pp. 4082-4088, December 1981.
7. F. T. S. Yu, S. L. Zhuang and S. T. Wu, "Source Encoding for Partial Coherent Optical Processing," Applied Physics, Vol. B27, pp. 99-104, February 1982.
8. S. T. Wu and F. T. S. Yu, "Visualization of Color Coded Phase Object Variation with Incoherent Optical Processing Technique," Journal of Optics, Vol. 13, pp. 111-114, May-June, 1982.
9. S. L. Zhuang and F. T. S. Yu, "Coherence Requirement for Partially Coherent Optical Information Processing," Applied Optics, Vol. 21, pp. 2587-2595, July 1982.
10. F. T. S. Yu and S. T. Wu, "Color Image Subtraction with Encoded Extended Incoherent Source," Journal of Optics, 13, 183 (1982).
11. S. L. Zhuang and F. T. S. Yu, "Apparent Transfer Function for Partially Coherent Optical Information Processing," Applied Physics, B28, 359-366, August, 1982.
12. Y. W. Zhang, W. G. Zhu, and F. T. S. Yu, "Rainbow Holographic Aberrations and Bandwidth Requirements," Applied Optics. 22, 164 (1983).
13. F. T. S. Yu, X. X. Chen, and S. L. Zhuang, "Progress Report on Archival Storage of Color Films with White-Light Processing Technique," submitted to Applied Optics.
14. T. H. Chao, S. L. Zhuang, S. Z. Mao and F. T. S. Yu, "Broad Spectral Band Color Image Deblurring," Applied Optics. 22, 1439 (1983).
15. F. T. S. Yu, Optical Information Processing, Wiley-Interscience, N.Y., 1983.

16. F. T. S. Yu, "Source Encoding, Signal Sampling and Filtering for White-Light Signal Processing," Proceedings of 10th International Optical Computer Conference, pp. 111-116, April 6-8, 1983.
17. X. J. Lu and F. T. S. Yu, "Restoration of Out-of-Focused Color Photographic Images," Optics Communications, Vol. 46, pp. 278-833, July (1983).
18. C. Warde, H. J. Caulfield, F. T. S. Yu and J. E. Ludman, "Real-Time Joint Spectral-Spatial Matched Filtering," Optics Communications, Vol. 49, pp. 241-244, March (1984).
19. F. T. S. Yu, "Source Encoding, Signal Sampling and Spectral Band Filtering for Partially Coherent Optical Signal Processing," Journal of Optics, Vol. 14, pp. 173-178, July-August (1983).
20. F. T. S. Yu, "Recent Advances in White-Light Optical Signal Processing," Conference on Laser and Electro-Optics, Cleo '83 Technical Digest, pp. 28-30, May (1983).
21. F. T. S. Yu, X. X. Chen and T. H. Chao, "Density Pseudocolor Encoding with Three Primary Colors," Journal of Optics, Vol. 15, pp. 55-58, March-April (1984).
22. F. T. S. Yu, S. L. Zhang and K. S. Shaik, "Noise Performance of a White-Light Optical Signal Processor: Part I, Temporally Partially Coherent Illumination, Journal of the Optical Society of America A, Vol. 1, pp. 489-494, May (1984).
23. F. T. S. Yu, F. K. Hsu and T. H. Chao, "Coherence Measurement of a Grating-Based White-Light Optical Signal Processor," Applied Optics, Vol. 23, pp. 333-340, January (1984).
24. F. T. S. Yu, "Advances in White-Light Optical Signal Processing," Proceedings on Optical Information Processing Conference II, NASA CP-2303 Conference publication, pp. 53-69, August (1983).
25. S. L. Zhuang, "Coherence Requirements, Transfer Functions and Noise Performance of a Partially Coherent Optical Processor," Ph.D. Dissertation, Pennsylvania State University, University Park, PA, 1983.
26. T. H. Chao, "A Grating-Based White-Light Optical Signal Processor," Ph.D. Dissertation, Pennsylvania State University, University Park, PA, 1983.

27. X. J. Lu, "Pseudocolor Encoding with White-Light Processing System," *Optics Communications*, pp. 13-16, November (1983).
28. J. E. Ludman, B. Javidi, F. T. S. Yu, H. J. Caulfield and C. Warde, "Real-Time Colored-Pattern Recognition," *SPIE Proceedings of Spatial Light Modulators and Applications*, Vol. 465, pp. 143-149, January 1984.
29. F. T. S. Yu, X. X. Chen and S. L. Zhuang, "Progress Report on Archival Storage of Color Films Utilizing a White-Light Processing Technique," *Journal of Optics*, Vol. 16, pp. 59-61, January-February (1985).
30. F. T. S. Yu, T. N. Lin and K. B. Xu, "White-Light Optical Speech Spectrogram Generation," *Applied Optics*, Vol. 24, pp. 836-841, March (1985).
31. F. T. S. Yu and G. W. Petersen, "A Low-Cost High-Quality Pseudocolor Encoder for Remote Sensing Applications," submitted to *Photogrammetric Engineering and Remote Sensing*.
32. B. Javidi and F. T. S. Yu, "Optics at Pennsylvania State University," *Optical Engineering*, Vol. 23, SR, pp. 068-071, May/June (1984).
33. F. T. S. Yu, X. J. Lu and M. F. Cao, "Applications of Magneto-Optic Spatial Light Modulator to White-Light Optical Processing," *Applied Optics*, Vol. 23, pp. 4100-4104, November (1984).
34. F. T. S. Yu and X. X. Chen, "Solar Optical Processing," *Optics Communications*, Vol. 51, pp. 377-381, October (1984).
35. F. T. S. Yu and H. Mueller, "A Low-Cost White-Light Optical Processor," *IEEE Transaction of Education* (in press).
36. F. T. S. Yu, "Recent Advances in White-Light Image Processing," *ICO-13 Conference Digest on "Optics in Modern Science and Technology"*, pp. 412-413, August (1984).
37. F. T. S. Yu and X. X. Chen, "A Low-Cost White-Light Pseudocolor Encoder for Astronomical Imaging Applications," *International Conference on "Progress in Optical Physics"*, Melbourne, Australia, August 15-17, 1984.
38. F. T. S. Yu, L. N. Zheng and F. K. Hsu, "Noise Measurement of a White-Light Optical Signal Processor," *Applied Optics*, Vol. 24, pp. 173-178, January (1985).
39. H. M. Mueller, "A Low-Cost White-Light Optical Processor," M.S. Dissertation, Pennsylvania State University, University Park, PA, 1984.
40. F. T. S. Yu and F. K. Hsu, "White-Light Fourier Holography," *Optics Communications*, Vol. 52, pp. 384-388, January (1985).

41. F. T. S. Yu and F. K. Hsu, "Generation of Broadband Fourier Holograms," SPIE Proceedings on "Application of Holography," Vol. 523, pp. 319-323, January (1985).
42. F. T. S. Yu, White-Light Optical Signal Processing, Wiley-Interscience, NY, May 1985.
43. F. T. S. Yu, "Garden of White-Light Optical Signal Processing," Optics News, Vol. 11, pp. 5-8, May (1985)(invited).
44. F. K. Hsu, "White-Light Fourier Transform Holography," M.S. Dissertation, Pennsylvania State University, University Park, PA, 1985.
45. M. S. Dymek, "Color Image Processing with Computer-Generated Spatial Filters in a Dispersed White-Light Optical System," Ph.D. Dissertation, Pennsylvania State University, University Park, PA, 1985.

END

DTIC

9-86